People's Democratic Republic of Algeria

Ministry of Higher Education and Scientific Research

University of Ghardaîa

Faculty of Natural and Life Sciences and Earth Sciences

Department of Biology

IN VIEW OF OBTAINING THE DEGREE OF

MASTER

Field of study: Biological Sciences

Option: Applied Biochemistry

By:
Abderrezek ELALOUANI

In silico study of the anti-xanthine oxidase activity of certain metabolites derived from marine sponges

---

Publicly defended, on the 16/06/2025, before a jury composed of

Mr. Mahfoud BAKLI	Univ. Ghardaïa	President
Mr. Zineddine BENBEKHTI	Univ. Ghardaïa	Reviewer
Mr. Abderahmane LINANI	Univ. Ghardaïa	Supervisor
Mrs. Leila BOU-SALAH	ENS. Laghouat	Co-supervisor

Academic year: 2024/2025

Acknowledgements

First and foremost, I would like to express my deepest gratitude to Almighty God for granting me the health, strength, and determination to begin and complete this work.

I extend my heartfelt thanks to Dr. Abderahmane LINANI, my supervisor, for his unwavering support and invaluable guidance throughout the course of this study. His expertise, dedication, and insightful advice were instrumental in shaping and completing this dissertation.

My sincere appreciation also goes to Dr. Leila BOU-SALAH, co-supervisor, for her support and thoughtful guidance. Her constructive suggestions and active involvement greatly enriched this research and contributed significantly to its quality.

I would also like to thank the members of the jury for kindly accepting to evaluate my dissertation. Their careful reading, valuable feedback, and insightful remarks will be of great benefit in improving the quality of this work.

I would also like to thank all the faculty members and professors of my university for the high-quality education and knowledge they have shared with me throughout my academic journey.

Dedication

Above all, I thank Almighty God for having given me the courage, strength, will and patience to carry out this work. I dedicate this thesis

To my dear parents, my mother and my father Who were my first support

To my dear brothers and sisters who have always supported and encouraged me during my years of study

To my best friends

To all my childhood friends and friends from my long school and university career.

To all my family

Abstract

This study investigates the therapeutic potential of five marine-derived metabolites as inhibitors of human xanthine oxidase (HXO), a critical enzymatic target in the treatment of gout an inflammatory disorder caused by the deposition of monosodium urate crystals in joints and surrounding tissues. Two alkaloids, Petrosin (Mol1) and Xestospongin D (Mol2), were selected from the marine sponge *Oceanapia sp*. A phenolic acid, Gentisic acid (Mol3), was obtained from *Hemimycale columella*. Additionally, two sesquiterpenoids, Sydonol (Mol4) and Aspergiterpenoid A (Mol5), were derived from a fungal strain (*Aspergillus sp*.) isolated from the sponge *Xestospongia testudinaria*. Molecular docking analysis using AutoDock Vina revealed that Mol1 and Mol2 exhibit the strongest binding affinities toward HXO, with binding energies of -11.5 kcal/mol and -8.8 kcal/mol, respectively significantly surpassing the reference drug allopurinol (-5.9 kcal/mol). Mol3, Mol4, and Mol5 also demonstrated enhanced binding stability compared to allopurinol. Complementary ADMT (absorption, distribution, metabolism, and toxicity) predictions indicated favorable pharmacokinetic properties and safety profiles, including low carcinogenic potential and minimal risk for cardiotoxicity. Collectively, these in silico findings underscore the promise of marine-derived metabolites, particularly Mol1 and Mol2, as novel HXO inhibitors that may lead to safer and more effective gout treatments. Further *in vitro* and *in vivo* validation is warranted to confirm these results.

Keywords: Gout, xanthine oxidase, marine-derived metabolites, alkaloids, molecular docking, ADMT, Petrosin.

Résumé

Cette étude évalue le potentiel thérapeutique de cinq métabolites dérivés de sources marines en tant qu'inhibiteurs de la xanthine oxydase humaine (XOH), une enzyme clé ciblée dans le traitement de la goutte, une maladie inflammatoire causée par le dépôt de cristaux d'urate monosodique dans les articulations et les tissus environnants. Deux alcaloïdes, la pétrosine (Mol1) et la xestospongine D (Mol2), ont été sélectionnés à partir de l'éponge marine *Oceanapia sp*. Un acide phénolique, l'acide gentisique (Mol3), a été isolé de *Hemimycale columella*. De plus, deux sesquiterpénoïdes, le sydonol (Mol4) et l'aspergitépénéoïde A (Mol5), proviennent d'une souche fongique (*Aspergillus sp*.) isolée de l'éponge *Xestospongia testudinaria*. L'analyse de docking moléculaire réalisée avec AutoDock Vina a révélé que Mol1 et Mol2 présentent les affinités de liaison les plus fortes avec la XOH, avec des énergies de liaison de -11,5 kcal/mol et -8,8 kcal/mol respectivement, surpassant largement la référence, l'allopurinol (-5,9 kcal/mol). Mol3, Mol4 et Mol5 ont également démontré une stabilité de liaison supérieure à celle de l'allopurinol. Les prédictions complémentaires ADMT (absorption, distribution, métabolisme et toxicité) ont indiqué des profils pharmacocinétiques et de sécurité favorables, incluant un faible potentiel carcinogène et un risque minimal de cardiotoxicité. Dans l'ensemble, ces résultats *in silico* soulignent le potentiel des métabolites marins, en particulier Mol1 et Mol2, comme inhibiteurs novateurs de la XOH, pouvant offrir des traitements plus sûrs et efficaces contre la goutte. Des validations complémentaires *in vitro* et *in vivo* sont nécessaires pour confirmer ces résultats.

Mots-clés : Goutte, xanthine oxydase, métabolites d'origine marine, alcaloïdes, docking moléculaire, ADMT, Petrosine.

ملخص

تُقيّم هذه الدراسة الإمكانات العلاجية لخمس مركبات مستخلصة من الكائنات البحرية كمثبطات لإنزيم الزانثين أوكسيداز البشري، وهو إنزيم رئيسي مستهدف في علاج مرض النقرس وهو اضطراب التهابي شائع يحدث نتيجة ترسيب بلورات يورات الصوديوم في المفاصل والأنسجة المحيطة بها. من الإسفنج البحري من نوع أوشيانابيا، تم اختيار مركبين من القلويات: بيتروسين (المركب 1) وزيستوسبونجين د (المركب 2). كما تم اختيار حمض فينولي وهو حمض جنتيسييك (المركب 3) من الإسفنج هيمايميكال كولوميلا. بالإضافة إلى ذلك، تم دراسة مركبين من مشتقات السسكويتيربينويد وهما سيدونول (المركب 4) والأسبرجيتربينويد أ (المركب 5)، وهما مستخلصان من فطر من جنس أسبرغيلوس تم عزله من الإسفنج زستوسبونجيا تيستوديناريا. أظهرت تحليلات الارتباط الجزيئي التي أجريت باستخدام برنامج أوتو دوك فينا أن المركبين 1 و 2 يمتلكان أعلى طاقات ارتباط مع إنزيم الزانثين أوكسيداز البشري، حيث بلغت طاقات الارتباط 11.5- و 8.8- كيلو كالوري/مول على التوالي، متفوقين بشكل كبير على الدواء المرجعي ألوبورينول (5.9- كيلو كالوري/ مول). كما أظهرت المركبات 3 و 4 و 5 ثباتاً أفضل في الارتباط مقارنة بالألوبورينول. كشفت التنبؤات المكملة لخصائص الامتصاص والتوزيع والتمثيل الغذائي والسمية عن مواصفات دوائية وسلامة واعدة، بما في ذلك احتمالية منخفضة للتسرطن ومخاطر ضئيلة على القلب. تُبرز هذه النتائج المحاكاة الحاسوبية الإمكانات الواعدة لهذه المركبات البحرية، وخصوصاً المركبين 1 و 2، كمثبطات جديدة لإنزيم الزانثين أوكسيداز البشري، مما قد يفتح آفاقاً لعلاجات أكثر أماناً وفعالية للنقرس. ومن الضروري إجراء دراسات إضافية مختبرية وحيوية لتأكيد هذه النتائج.

الكلمات المفتاحية: النقرس، إنزيم الزانثين أوكسيداز، المستقبلات البحرية، القلويدات، الارتباط الجزيئي، خصائص الامتصاص والتوزيع والتمثيل والسمية، بيتروسين.

List of figures

List of tables

List of abbreviations

A	B-D
ADMT: Absorption, distribution, metabolism, toxicity. **ADT**: AutoDock Tools. **ADV**: AutoDock Vina. **ATP**: Adenosine triphosphate. **ABC**: ATP-Binding cassette. **ACY**: Acetic acid. **ABCG2**: ATP binding cassette transporter subfamily G member 2.	**BBB:** Blood-Brain Barrier. **Caco-2**: Human Colon Carcinoma Cell stage 2. **CYP**: Cytochrome. **CKD**: Chronic Kidney Disease. **CT**: Computed Tomography. **DSV**: Discovery Studio Visualizer. **DECT**: Dual-Energy Computed Tomography.

E-I	L-N
FAD: Flavin Adenine Dinucleotide **GB:** Grid Box. **HERG:** Human Ether Related Gene. **HIA**: Human Intestinal Absorption. **HXO**: Human Xanthine Oxidase. **HIV**: Human Immunodeficiency Virus. **IL-1β**: Interleukin_1β.	**MRI**: Magnetic Resonance Imaging. **MSU**: Monosodium urate. **Mo**: Molybdenum. **MDCK**: Mandin Darby canine kidney cell. **MD**: Molecular Docking. **NSAIDs**: Non_steroidal anti-inflammatory drugs. **NAD**: Nicotinamide adenine dinucleotide. **NCBI:** National center for biotechnology information. **NMR:** Nuclear Magnetic Resonance **NIH:** National Institutes of Health. **NLRP3:** NOD-, LRR-, and pyrin domain-containing protein 3.

P-R	S-X
PDB: Protein Data Bank. **PDBQT**: Protein Data Bank, Partial Charge (Q), and Torsions (T). **P-gp**: P-glycoprotein. **PreADMET**: Prediction of Absorption, Distribution, Metabolism, Excretion, and Toxicity. **QSARs:** quantitative structure–activity relationships. **RCSB:** Research Collaboratory for Structural Bioinformatics.	**SDF**: Structure Data Format. **SLC22A12**: Solute carrier family 22 member 12. **SMILES**: Simplified Molecular Input Line Entry System. **UA**: Uric Acid. **URAT1**: Uric acid transporter1. **SUA**: Serum Uric Acid. **SDF**: Structure Data File. **SPECT**: Single Photon Emission Computed Tomography. **US**: Ultrasound. **XDH**: Xanthine Dehydrogenase. **XO**: Xanthine Oxidase.

Table of contents

INTRODUCTION

Gout has been recognized as an important medical condition since ancient times [1], frequently mentioned in early medical writings and linked to prominent historical figures [2]. Often called the "disease of kings," it was first noted by the Egyptians around 2640 B.C., and Hippocrates later described it as an illness of older men caused by indulgent lifestyles [3]. The term "gout" comes from the Latin *gutta*, meaning "drop," reflecting the medieval belief that an excess of bodily humors could drip into joints and cause inflammation [2]. This term was first recorded in the 13th century by the monk Randolphus of Bocking, who mistakenly grouped gout with other joint diseases like rheumatism [3]. A clearer distinction between gout and rheumatism was made in the 17th century by physician Thomas Sydenham, who suffered from both gout and kidney disease [3].

Gout is the most prevalent type of inflammatory arthritis and has a substantial impact on patients' quality of life [4]. It is caused by elevated levels of serum uric acid (SUA), a condition known as hyperuricemia [5], which plays a central role in the disease's onset. When SUA exceeds the solubility threshold in bodily fluids, monosodium urate (MSU) crystals begin to form and accumulate (> 7 mg/dL) around the joints [6]. This buildup triggers a range of clinical symptoms, including intense episodes of joint pain and inflammation most commonly in the big toe joint as well as chronic joint deterioration and the formation of tophaceous deposits in both joints and surrounding skin [7].

Currently, the primary approach to managing hyperuricemia in clinical settings involves decreasing uric acid (UA) production while also enhancing its excretion. As a result, targeting xanthine oxidase (XO) inhibition is considered an effective strategy for lowering UA levels [8].

Patients commonly receive non-steroidal anti-inflammatory drugs (NSAIDs) or colchicine to manage acute gout flares [9]. However, the long-term use of these medications is often associated with significant adverse effects. Therefore, identifying alternative therapeutic strategies is of considerable clinical importance [10]. Our research focuses on marine pharmacognosy, specifically exploring metabolites derived from marine sponges as potential

candidates for safer and more effective gout treatments **[11-13]**. As invertebrates, sponges produce a wide range of bioactive secondary metabolites that function as natural chemical defenses against predators and fouling organisms **[13]**. This remarkable biosynthetic capacity positions them as a valuable resource for drug discovery and pharmaceutical innovation **[14]**.

This study aims to identify novel anti-gout compounds by evaluating their inhibitory potential against human xanthine oxidase (HXO). This study investigates alkaloid, phenolic acid, and terpenoid compounds derived from marine sponges, specifically *Oceanapia sp., Hemimycale columella,* and *Xestospongia testudinaria*. The research methodology is based on the selection of compounds with favorable pharmacokinetic properties, particularly low predicted toxicity, assessed using the Pre-ADMET 2.0 server. Following this screening, molecular docking analysis were performed using AutoDock Vina and AutoDock Tools to estimate the binding affinities of the selected metabolites..

The study is organized into three main sections, structured as follows:

- **The first section** provides a concise literature review, establishing the foundational concepts underpinning this study. It begins with an overview of gout, addressing its etiology, clinical manifestations, diagnostic approaches, and current treatment strategies. The discussion then transitions to HXO, highlighting its relevance as a pharmacological target. This section also includes a brief overview of the taxonomy, geographical distribution, and morphological features of the marine sponges employed in the research.

- **The second section** details the experimental design, including the materials and methodologies utilized throughout the study. It is followed by a comprehensive presentation and analysis of the results, which are critically discussed to extract relevant scientific insights.

- **The final section** offers the conclusion and future perspectives, summarizing key findings and proposing potential directions for further investigation.

LITERATURE REVIEW

1. Gout

1.1 Definition

Gout is a metabolic condition marked by the buildup of monosodium urate crystals in joints and other body tissues **[15]**. This buildup results from persistent hyperuricemia when SUA levels exceed 6.8 mg/dL, the point at which urate becomes insoluble and crystals begin to form (figure 1). The presence of these crystals triggers a pronounced inflammatory reaction, causing sudden and painful arthritis flare-ups **[16]**. Gout is strongly linked to abnormalities in purine metabolism, with elevated UA levels being a key factor in the development of the disease **[17]**.
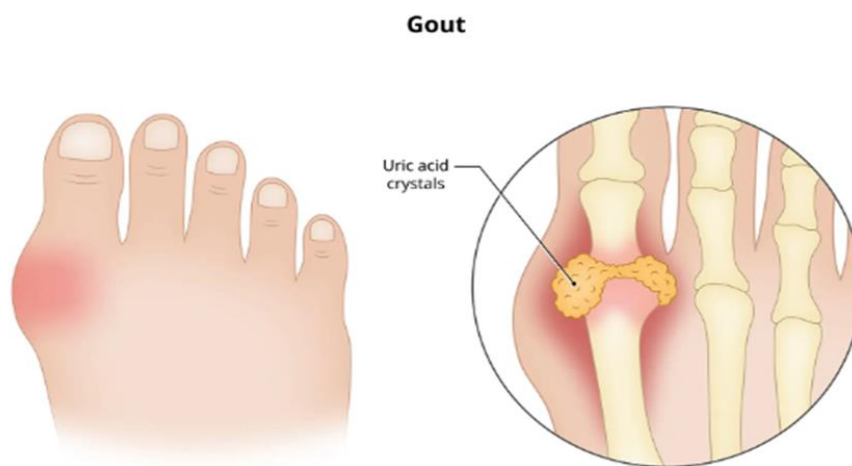
FIGURE 1: Deposition of UA crystals **[18]**.

1.2 Causes and factors

Gout primarily results from chronic hyperuricemia **[5]**, which occurs when there's an imbalance between the body's production and excretion of UA **[19]**. This condition can be caused by either increased purine degradation or decreased elimination of UA, particularly through the kidneys **[20]**. Lifestyle factors play a significant role, with diets high in purine-rich foods like red meat and beverages high in fructose (which is metabolized into purines) contributing to elevated UA levels **[21]**. Alcohol further aggravates this by adding purines and affecting metabolism **[21]**. Other contributors include genetic factors, obesity, and certain medications especially diuretics **[22]**. Chronic conditions such as high blood pressure, kidney dysfunction, and metabolic syndrome also raise the risk of developing gout **[22]**.

- **Endogenous metabolic disturbances such as tumor lysis syndrome**: Rapid destruction of tumor cells releases nucleic acids, which are metabolized into UA, leading to hyperuricemia. This is particularly relevant during cancer treatments [23].

  Fasting and Starvation: Periods of fasting can increase purine turnover, resulting in elevated UA levels, thereby increasing the risk of gout attacks [24].

- **Poor UA elimination, especially through the kidneys**, is another major factor. Although the kidneys and gut normally filter and secrete UA, about 90% is reabsorbed via URAT1 transporters a process influenced by kidney health, sodium balance, alcohol intake, and diuretics like thiazides and furosemide [22].

- **Genetics play a key role** as well. Variations in genes related to urate transport (SLC22A12, ABCG2) or purine metabolism can affect UA levels. Furthermore, humans lack the enzyme uricase, which would otherwise convert UA into more soluble allantoin, promoting crystal buildup [25].

- **Environmental triggers influencing gout:** Emerging research indicates that environmental factors, including air pollution, temperature fluctuations, and seasonal changes, may influence inflammatory pathways and oxidative stress, potentially triggering or exacerbating gout episodes [26].

While elevated UA is necessary for gout to occur, not everyone with hyperuricemia develops the condition crystal formation in joints is also required. Gout is more common in men, possibly due to hormonal differences, and its incidence increases with age.

- **Comorbidities like obesity, cardiovascular disease, and kidney problems** are strongly associated with both hyperuricemia and gout. Additionally, new research suggests that environmental triggers such as air pollution, temperature changes, and seasonal variations may influence inflammation and oxidative stress, potentially initiating or worsening gout episodes, although the exact biological mechanisms are still being studied [27].

1.3   The crystallization of monosodium urate

As UA levels increase and begin to build up in joints and soft tissues, a process called nucleation begins [28]. During nucleation, dispersed UA molecules cluster together to initiate crystal formation. UA, being a weak acid, typically combines with sodium and water to form MSU [29].

MSU crystals are needle-shaped (figure 2) and consist of stacked purine rings. Their charged surfaces allow them to interact with cell membranes and circulating molecules, often-triggering inflammation [30]. The development of these crystals is influenced by factors such as body temperature, synovial fluid pH, water and electrolyte levels, and structural proteins like collagen [31].

These crystals can form larger aggregates called tophi and provoke acute gout attacks, which involve severe joint pain, swelling, redness, and inflammation commonly affecting the big toe, midfoot, ankle, or fingers [32]. This inflammatory reaction is mainly driven by the innate immune system, especially macrophages and neutrophils. A key mechanism in this response is the activation of the NLRP3 inflammasome, which promotes the production of inflammatory molecules like interleukin-1β (IL-1β) [18].
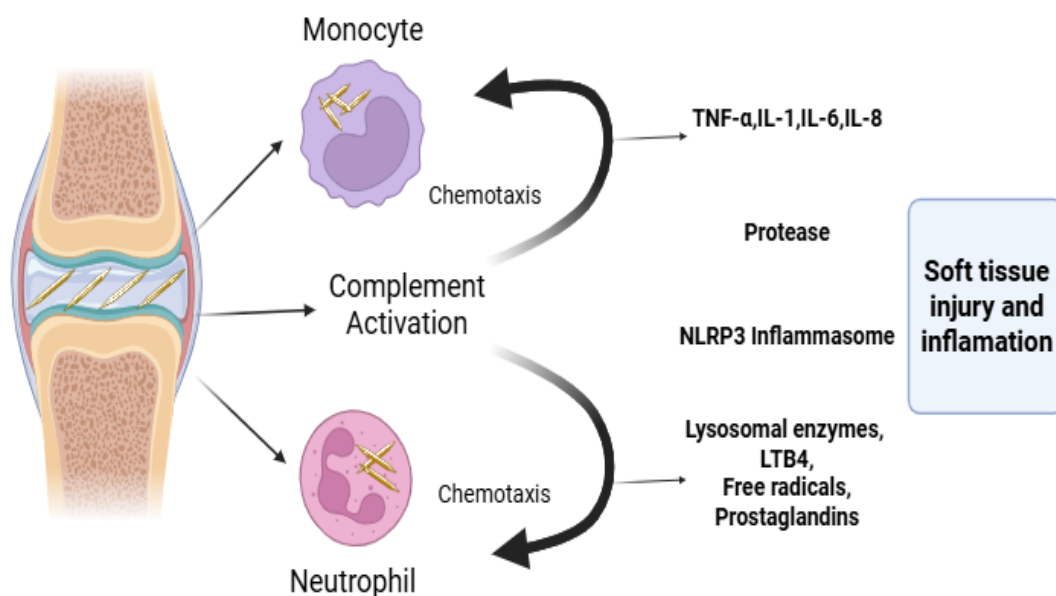
FIGURE 2: Pathogenesis of hyperuricaemia and an acute gouty arthritis [18].

1.4   Symptoms

In individuals with gout, the clinical course often progresses from asymptomatic hyperuricemia to symptomatic episodes characterized by crystal-induced joint inflammation. As MSU crystals accumulate, they may eventually provoke acute flares and form visible tophi (figure 3) **[32]**. These episodes involve significant joint inflammation **[18]**. Commonly involved sites include the metatarsophalangeal joint, midfoot, ankle, fingers, and upper limbs **[33]**. Additional symptoms may include skin peeling or flaking due to swelling, and in advanced stages, joint erosion and deformity. Between flares, patients experience intercritical periods symptom-free intervals during which urate deposition may continue unnoticed. As the condition progresses, these intervals often become shorter. If left untreated, repeated attacks and chronic inflammation may result in lasting joint pain, stiffness, and irreversible structural damage, marking the chronic phase of the disease **[34]**.

FIGURE 3: Chronic gout with tophi present in the hands and along the Achilles tendon. **[34]**.

1.5   Diagnosis and treatments

Diagnosis of gout usually begins with a detailed review of the patient's medical history and a comprehensive physical exam. Additionally, blood tests may be conducted to measure UA levels, aiding in the diagnostic process **[35]**. If the diagnosis of gout remains uncertain or incomplete, joint aspiration and synovial fluid microscopy should be considered as important diagnostic tools (figure 4). These procedures help detect MSU crystals, providing a more definitive confirmation of gout **[36]**.

Identifying MSU crystals can be challenging, as joint aspiration and synovial fluid analysis require specialized expertise and equipment that may not always be accessible, especially in primary care settings. As a result, imaging techniques play a crucial role in diagnosing gout, particularly for patients with uncertain or inconclusive clinical findings [37].
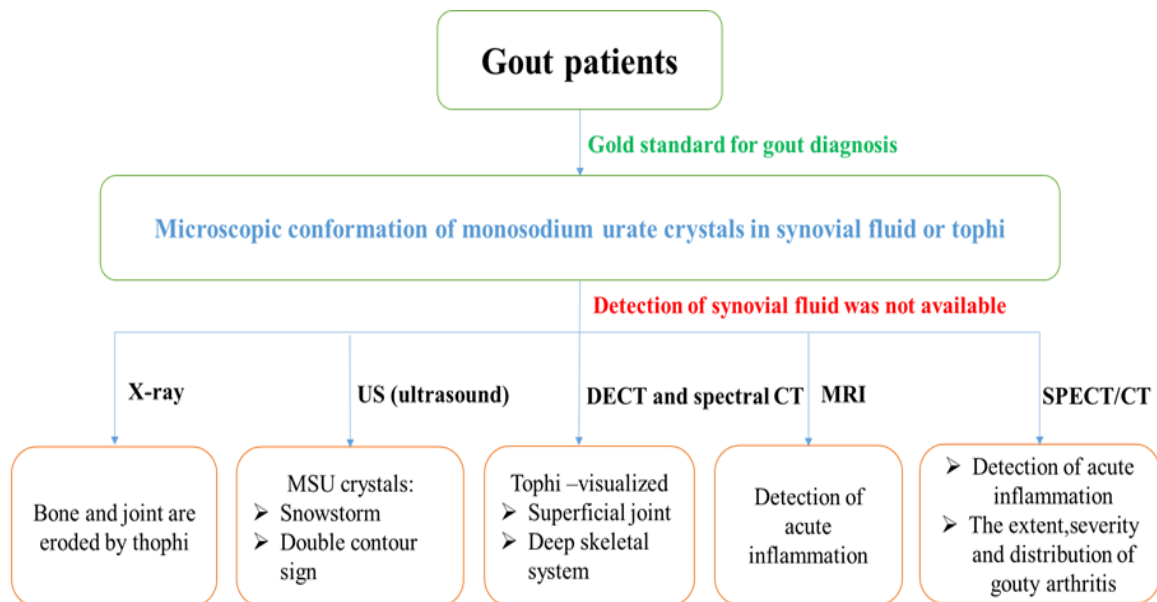
FIGURE 4: Gout imaging flowchart.
MRI: magnetic resonance imaging; **MSU**: monosodium urate monohydrate; **DECT**: dual energy computed tomography; **US**: ultrasound; **SPECT**: single photon emission computed tomography; **CT**: computed tomography.

The treatment of gout involves the use of XO inhibitors (table 1), which target this enzyme as the primary therapeutic approach for managing both gout and hyperuricaemia. By inhibiting XO, these medications effectively reduce the production of UA, helping to prevent flare-ups and complications associated with elevated UA levels [38]. Gout treatment can be highly effective. It generally involves two key components:

- **Managing acute flare-ups:** Treatment during a gout attack focuses on relieving symptoms like pain, swelling, and inflammation (table 1). The goal is to ease discomfort during the episode, rather than to lower UA levels or prevent future attacks. This approach does not tackle the root cause of gout.

- **Preventing future flare-ups:** Long-term management involves urate-lowering therapies, which work to decrease UA levels in the body. These medications help

dissolve existing crystals and prevent new ones from forming, addressing the underlying cause of gout and reducing the likelihood of recurrent attacks and joint damage **[39]**.

TABLE 1: Drugs indicated in the treatment of gout **[39]**.

Class	Drug (Brand)	Common Dosing
Urate-Lowering Therapy		
Xanthine oxidase inhibitors	Allopurinol (Zyloprim)	Starting dose: 100 mg/day (all patients); 50 mg/day (stage 4 CKD or worse) Dose titration: Titrate to doses >300 mg/day even in renal patients; doses >300 mg/day may be required for most patients. Max daily dose is 800 mg
	Febuxostat (Uloric)	Starting dose: 40 mg/day Dose titration: Increase to 80 mg/day after 2-4 weeks
Uricosuric agents	Probenecid (Benemid)	Starting dose: 250 mg/day Dose titration: Increase by 500 mg per month to a max dose of 2-3 g/day (2 divided doses) in patients with normal renal function
Uricase agents	Pegloticase (Krystexxa)	Dose: intravenous infusion 8 mg every 2 weeks
Acute Gout Attack Prophylaxis During Initiation of Urate-Lowering Therapy		
Antigout agents	Colchicine (Colcrys)	0.6 mg orally once or twice daily as tolerated
	Probenecid/colchicine (Col-Benemid)	500 mg/0.5 mg once daily for 7 days, then 500 mg/0.5 mg twice daily thereafter
NSAIDS	Naproxen	250 mg orally twice daily

NSAIDS: non-steroidal anti-inflammatory drugs   **CKD:** Chronic Kidney Disease

2. Xanthine oxidase

Xanthine oxidase is the terminal enzyme in human purine catabolism, catalyzing the sequential hydroxylation of hypoxanthine to xanthine and then xanthine to UA **[40]**. This enzyme is essential for purine metabolism and is conserved across a wide range of organisms. One of the earliest successful purifications of XO was reported in 1924 by Dixon and Thurlow, who isolated the enzyme from cow's milk. The enzyme exists in two interchangeable forms. One form acts as a dehydrogenase, using NAD as the final electron acceptor from the flavin site. The other form functions as an oxidase, where oxygen (O_2) serves as the electron acceptor instead **[41]**.

2.1. Structure

Xanthine oxidase is homodimeric enzyme with a total molecular weight of about 300 kDa. Each subunit is made up of a single polypeptide chain containing approximately 1,332 amino acids (figure 5). These subunits are equipped with several cofactors: one molybdopterin (Mo-pt), two 2Fe-2S clusters, and one FAD. These cofactors are located within distinct structural domains of the enzyme **[42]**:

- **The C-terminal domain, weighing approximately 85 kDa**.

- **The N-terminal domain, around 20 kDa**.

- **The intermediate domain, roughly 40 kDa**.

Each domain plays a specific role in the enzyme's structure and function.
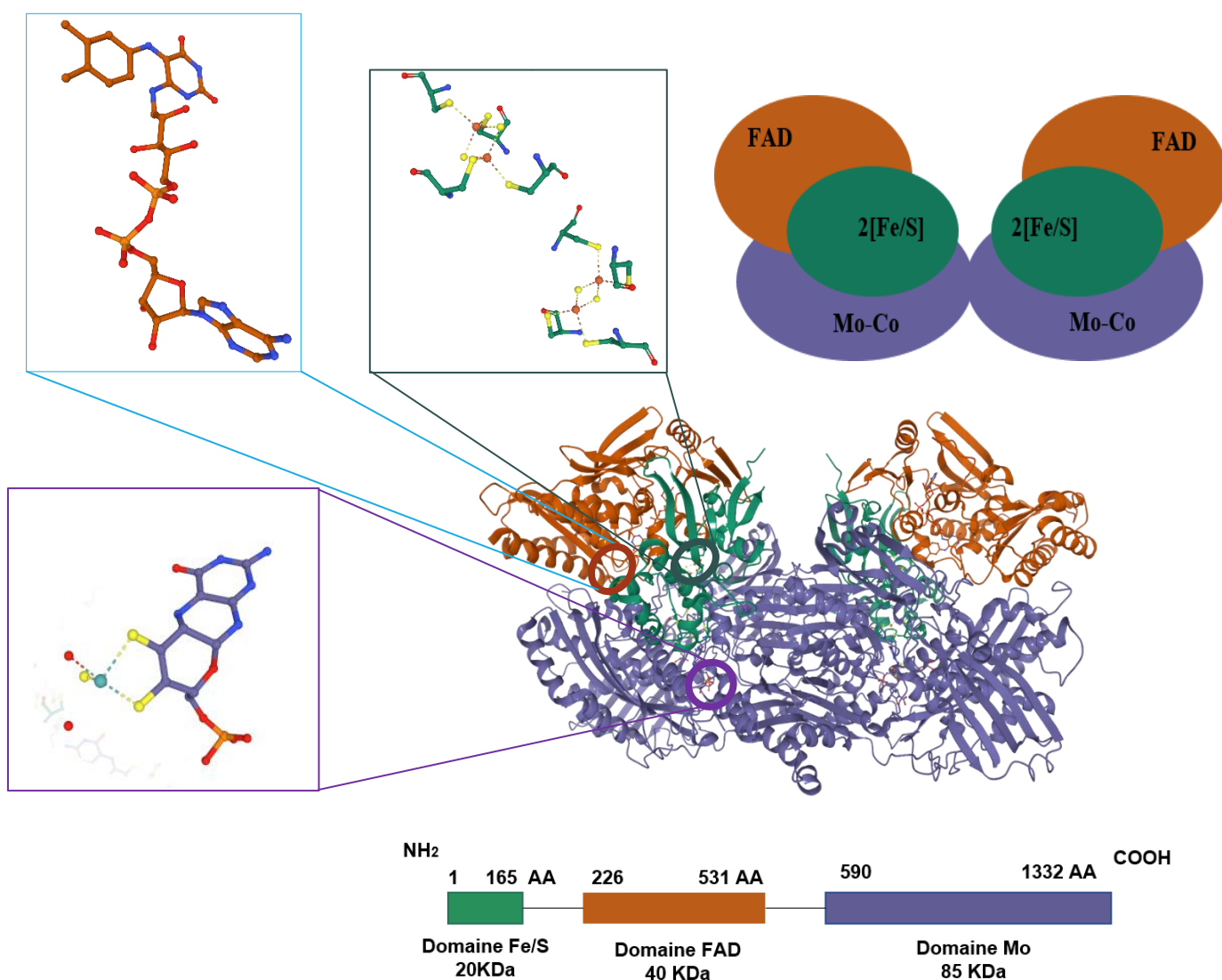
FIGURE 5: The 3D structure of xanthine oxidase.

2.2. Reaction mechanism

The catalysis is activated by a nucleophilic attack via the molybdenum center Mo (VI) Mo-OH on the C-8 carbon of the xanthine and in the presence of the catalytic amino acid Glu1261, which simultaneously leads to the reduction of Mo (VI) to Mo (IV). The first step consists in a reoxidation of the molybdenum center (figure 6) by electron transfer to Glu1261 of the active site, accompanied by the protonation of the Mo-SH bond, the second step consists in the deprotonation of the Mo-SH bond to Mo=S, the third step consists in regenerating the Mo-OH group of the molybdenum system (Mo (VI)) and releasing a new product which is the UA, consequently Glu1261 returns to its original ionic form. Finally, the fourth step will repeat the cycle [43].
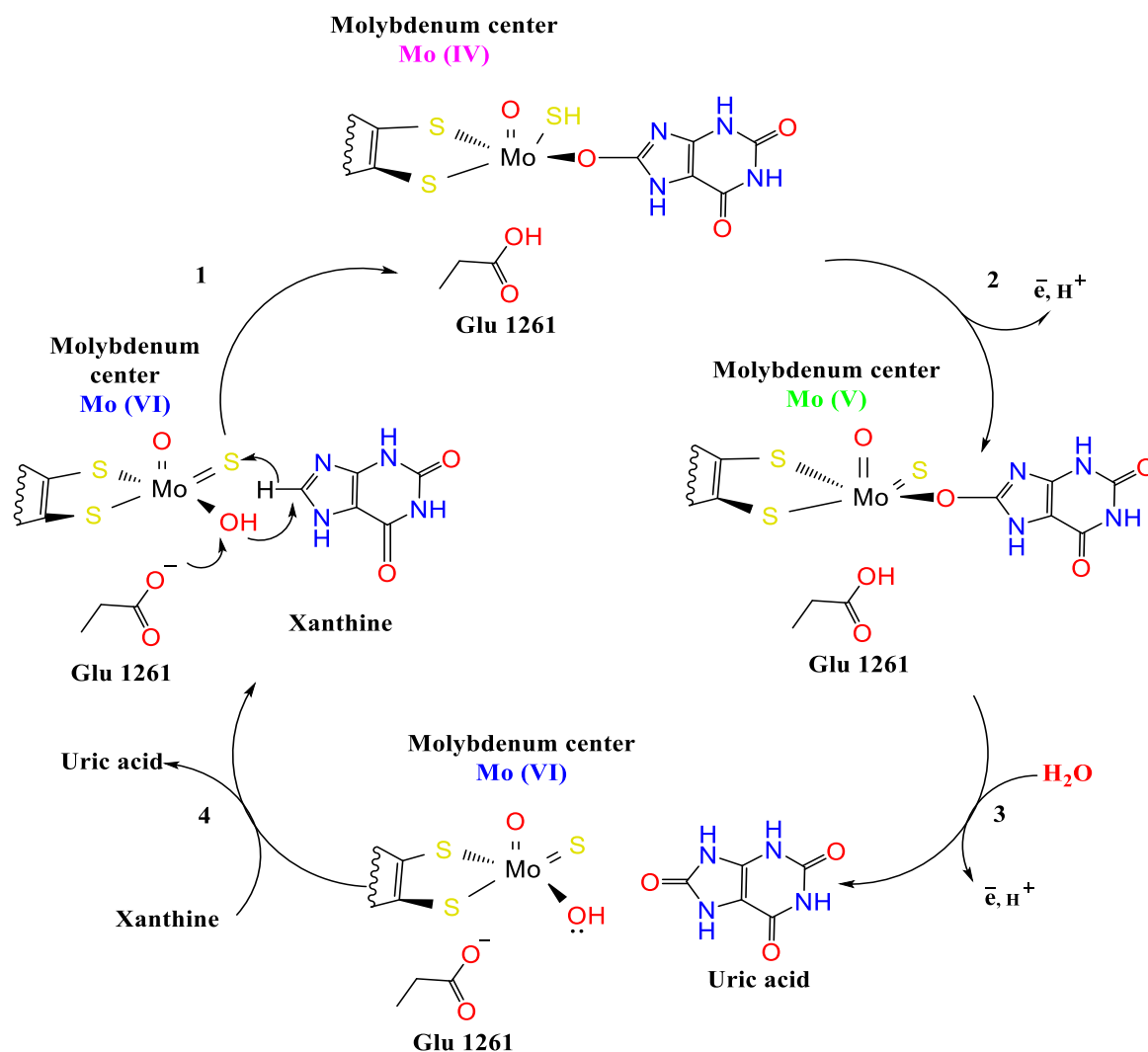
FIGURE 6: Scheme of the catalytic mechanism of xanthine oxidase [43].

2.3. The different forms of xanthine oxidase

Xanthine oxidase exists in different forms [40], primarily as xanthine oxidase abbreviated XO and xanthine dehydrogenase abbreviated XDH. These two forms are interconvertible and play a crucial role in purine metabolism: XO is the predominant form found in biological fluids such as plasma and milk [44]. XDH primarily utilizes NAD^+ as its oxidation substrate, facilitating electron transfer for purine metabolism. However, it can also interact with molecular oxygen (O_2, though less efficiently). In contrast, XO is unable to use NAD^+ and relies exclusively on O_2 as its electron acceptor, producing reactive oxygen species alongside UA formation [42].

3. Studied sponges

For centuries, alkaloids have played a crucial role in human history due to their potent biological activities and diverse chemical structures. These naturally occurring compounds, primarily derived from plants, have been extensively utilized in traditional and modern medicine, as well as in agriculture and biotechnology, for their therapeutic, insecticidal, and antimicrobial properties [45]. In recent decades, the marine environment has emerged as a prolific and relatively untapped source of novel bioactive alkaloids and other secondary metabolites. Marine organisms, especially invertebrates such as sponges, tunicates, and mollusks, have demonstrated remarkable chemical diversity [46].

A comprehensive study examining marine natural products from 1985 to 2012 revealed that nearly 75% of newly discovered marine-derived compounds originated from invertebrates [47]. Among these, sponges (phylum Porifera) stood out as the richest reservoir of bioactive molecules, largely due to their unique symbiotic relationships with microorganisms and their exposure to complex ecological pressures in marine habitats. These findings underscore the immense potential of marine invertebrates as sources of pharmacologically active alkaloids and highlight the importance of continued exploration of ocean biodiversity for drug discovery and development.

In this study, we focused on three sponge species known for their potential to produce diverse secondary metabolites:

- *Oceanapia sp* (Figure 7).

- *Hemimycale columella* (Figure 8).

- *Xestospongia testudinaria* (Figure 9).

Their taxonomic classification and geographical distribution and morphology were obtained from reliable sources, including the *Sponge Guide* **[48]**, *World Porifera Database* **[49]**, *Florent's Guide To The Florida, Bahamas & Caribbean Reefs* **[50]** and the *iNaturalist Guide* **[51]**.

3.1. Oceanapia sp

Common Name: Buried sponge.

3.1.1. Taxonomy

Kingdom	*Animalia*
Phylum	*Porifera*
Class	*Demospongiae*
Order	*Haplosclerida*
Family	*Phloeodictyidae*
Genus	*Oceanapia*

3.1.2. Geographical distribution and morphology

Oceanapia sp. is a marine sponge genus with a broad distribution, including regions such as the Caribbean, the Bahamas, and parts of the Pacific Ocean, notably near Micronesia and Western Australia. Members of this genus are typically found at depths ranging from 18 to 130 feet (approximately 5.5 to 40 meters) **[50]**. These sponges exhibit a distinctive morphology characterized by a buried, bulbous base from which one or more slender, tubular projections called fistules emerge through the substrate. Each fistule terminates in a fragile, cap-like structure known as a capitum. The sponge's surface is often hispid and may be covered by other organisms or sediment **[52]**. The skeletal structure of *Oceanapia sp*. comprises oxeas smooth,

straight to slightly curved megascleres with variably shaped ends (acerate, hastate, or blunt) measuring approximately 125 to 408 µm in length and 2 to 14 µm in thickness. Microscleres, when present, include sigmas or toxas, contributing to the sponge's structural integrity **[53]**.

Ecologically, *Oceanapia sp*. plays a role in benthic environments, often inhabiting sandy or sediment-rich substrates. Notably, certain species within this genus produce secondary metabolites, such as kuanoniamines C and D, which have been shown to deter predation by reef fishes, indicating a chemical defense mechanism **[52]**.

Oceanapia sagittaria
Location: Lembeh Strait, Indonésie
Photographer: Sylvain le bris
Picture taken on: 11-07-2017 07:59

Oceanapia polytuba
Location: Sechelt Inlet, BC, Canada.
Photographer: Neil McDaniel
Picture taken on: 09-01-2015 15:57

FIGURE 7: Photos represents *Oceanapia genus* (obtained from *iNaturalist*).

3.1.3. Derived metabolites

The genus *Oceanapia* represents a valuable source of chemically diverse and biologically active secondary metabolites with significant pharmacological potential. Among these are quinolizidine alkaloids, including petrosin and xestospongins, which have been isolated from *Oceanapia* and related marine sponges **[54]**. Petrosin, a bis-quinolizidine alkaloid first identified from *Petrosia similis*, and its derivative petrosin-A, exhibit notable anti-HIV activities by inhibiting early steps of HIV replication (IC_{50} values of 41.3 µM and 52.9 µM, respectively) as well as HIV-1 reverse transcriptase (10.6 µM and 14.8 µM) **[55]**. Xestospongins, a series of bis-1-oxaquinolizidine alkaloids, show diverse bioactivities such as

vasodilation, cytotoxicity against cancer cell lines (HepG-2, HL-60, LU-1, MCF-7, SK-Mel-2) with IC_{50} values between 0.43 and 1.02 μM, and moderate antimicrobial effects **[56]**.

Other notable alkaloids from *Oceanapia* include kuanoniamines, which possess antimicrobial and anticancer properties **[57]**, petrosamine B, an inhibitor of the *Helicobacter pylori* enzyme aspartyl semialdehyde dehydrogenase **[58]**, and oceanapamines, which demonstrate strong antiparasitic and anti-inflammatory activities **[59]**. Given their diverse and potent biological effects, petrosin and xestospongins, isolated from *Oceanapia*, were selected in this study as promising candidates for investigation as potential gout inhibitors.

3.2. *Hemimycale columella*

Common Name: Crater sponge

3.2.1. Taxonomy

Kingdom	*Animalia*
Phylum	*Porifera*
Class	*Demospongiae*
Subclass	*Heteroscleromorpha*
Order	*Poecilosclerida*
Family	*Hymedesmiidae*
Genus	*Hemimycale*
Species	*Hemimycale columella*

3.2.2. Geographical distribution and morphology

Hemimycale columella is a brightly colored encrusting sponge species widely distributed across the eastern North Atlantic and the Mediterranean Sea. It has been recorded along the western and southern coasts of the British Isles, the Bay of Biscay, the Azores, and extensively throughout the western Mediterranean, including the Adriatic and Aegean Seas **[60]**. Typically found at depths ranging from the shallow subtidal zone down to approximately 100 meters, *Hemimycale columella* favors rocky substrates in moderately sheltered environments. Morphologically, the sponge forms cushion-like or encrusting growths with a smooth to slightly hispid surface and scattered oscula. Fresh specimens are usually vivid red, orange, or pink,

although this coloration often fades upon preservation **[61]**. The skeletal structure consists of plumose tracts of styles, supported by microscleres such as sigmas and rhabdostyles, which are key diagnostic features used for taxonomic identification **[62]**. The combination of its widespread distribution and distinct morphological features has made *Hemimycale columella* an important species in benthic community studies and marine sponge taxonomy.

FIGURE 8: Photo represents *Hemimycale columella* (obtained from *iNaturalist*).
Location: Olbia-Tempio, Sardegna, IT. **Photographer**: Frédéric ANDRE.
Picture taken on: Juillet 1, 2019 09:49.

3.2.3. Derived metabolites

Hemimycale columella has been recognized as a prolific source of bioactive secondary metabolites, particularly phenolic compounds and other small molecules with significant pharmacological potential. Among its identified metabolites are various phenolic acids, brominated alkaloids, and glycosylated derivatives that exhibit antimicrobial, antioxidant, and anti-inflammatory activities **[63, 64]**. One notable compound isolated from *Hemimycale columella* is gentisic acid 2-O-β-glucoside, a phenolic glycoside with reported antioxidant and enzyme-inhibitory properties **[64]**. In the present study, gentisic acid 2-O-β-glucoside was selected for its potential as a XO inhibitor, a key therapeutic target in the treatment of gout.

This selection was based on both its natural occurrence in *Hemimycale columella* and its structural suitability for interfering with UA biosynthesis pathways. The inclusion of this compound underscores the relevance of marine sponges such as *Hemimycale columella* as reservoirs of novel lead molecules for drug discovery against metabolic disorders.

3.3. Xestospongia testudinaria

Common Name: Giant barrel sponge.

3.3.1. Taxonomy

Kingdom	*Animalia*
Phylum	*Porifera*
Class	*Demospongiae*
Order	*Haplosclerida*
Family	*Petrosiidae*
Genus	*Xestospongia*
Species	*Xestospongia testudinaria*

3.3.2. Geographical distribution and morphology

Xestospongia testudinaria, commonly referred to as a giant barrel sponge, is a prominent member of coral reef ecosystems throughout the Indo-Pacific region. Its distribution spans from the Red Sea and East African coast to Southeast Asia, the Philippines, Indonesia, and northern Australia, including the Great Barrier Reef **[65]**. It typically inhabits shallow reef slopes and fore-reef areas, ranging from 5 to 30 meters in depth, where it plays an essential role as a benthic filter feeder and habitat-forming organism. Morphologically, *Xestospongia sp* forms large, vase or barrel-shaped bodies, often exceeding 1.5 meters in diameter and height. Its thick, leathery walls exhibit a reddish to brownish-purple coloration, influenced by its dense and diverse microbial communities **[66]**. A single, large osculum at the top allows for the expulsion of filtered water. The sponge's skeleton is composed of siliceous spicules and spongin fibers, which provide structural support. Due to its size, longevity, and high microbial abundance, *Xestospongia sp* serves as a model organism in studies of sponge-microbe symbiosis, reef health, and the effects of climate change on reef ecosystems **[67]**.

FIGURE 9: Photo represents *Xestospongia testudinaria* (obtained from *iNaturalist*).
Location: Thailand. **Photographer**: Mike Morrison.
Picture taken on: Mai 9, 2025 08:08 PM.

3.3.3. Derived metabolites

Xestospongia testudinaria is a prolific source of structurally diverse and biologically potent secondary metabolites. Among the notable compounds isolated from this species is testusterol, a novel sterol exhibiting strong antibacterial activity against both Gram-positive and Gram-negative bacteria, with IC_{50} values below 12.0 nM [68]. Another sterol derivative, xestosterol-3-palmitate, has been identified from Red Sea specimens and contributes to the sponge's cytotoxic properties [69]. In addition, the sponge produces nonanedioic acid (azelaic acid), known for its bactericidal, anti-inflammatory, and antioxidant activities [70]. Tetradecanoic acid (myristic acid), also present, has shown significant larvicidal effects against mosquito species such as *Aedes aegypti* and *Culex quinquefasciatus* [70]. Notably, a bioactive peptide derived from *Xestospongia testudinaria* has demonstrated selective cytotoxicity toward human cervical cancer (HeLa) cells while sparing normal human embryonic kidney (HEK 293) cells [71]. Furthermore, the fungal strain *Aspergillus sp.*, isolated from the inner tissue of a freshly collected *Xestospongia testudinaria* specimen by Dan Li *et al.*, [72] has been a source of

additional bioactive compounds. In our study, we selected two sesquiterpenoids (Aspergiterpenoid A and sydonol) from this fungal isolate for their therapeutic potential. These findings highlight *Xestospongia testudinaria*, along with its associated microbial symbionts, as a valuable reservoir of pharmacologically active molecules with promising applications in gout therapies.

MATERIALS AND METHODS

1. Databases and webservers

1.1. Protein Data Bank (PDB)

The Protein Data Bank (PDB), founded in 1971 by a group of structural biologists, was the first publicly accessible repository (https://www.rcsb.org/) for biological data (figure 10). Initially focused on structural data, the archive has since broadened its scope to include data from macromolecular crystallography, NMR spectroscopy, and cryo-electron microscopy. To accommodate this expansion, advanced systems for data submission, validation, curation, storage, and dissemination were implemented. Active engagement from the scientific community has ensured the platform meets the needs of both data contributors and users.

Currently, the PDB holds more than 236,970 experimentally resolved structures (Figure 10), including proteins, nucleic acids, molecular complexes, and their interactions with small molecules. Impressively, maintaining this resource costs only about 1% of the total expense involved in determining these structures. The PDB has played a pivotal role in promoting progress across the natural and biomedical sciences, notably supporting the development of AI-driven 3D protein structure prediction tools such as AlphaFold2, RoseTTAFold, and OpenFold [73].
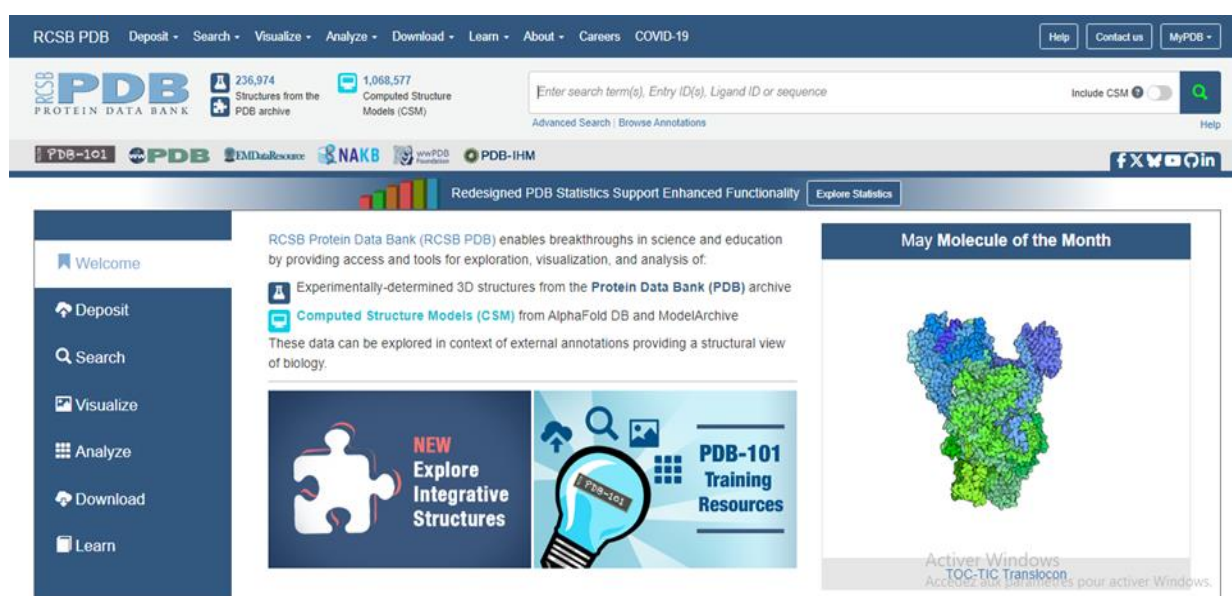
FIGURE 10: Latest view of the RCSB PDB homepage, accessed on May 10, 2025.

1.2. Pubchem

PubChem is a free, open-access chemical database (https://pubchem.ncbi.nlm.nih.gov/) maintained by the NCBI (NIH), providing extensive data on small molecules and their biological activities (figure 11). It aggregates information from over a thousand sources, including research institutions, government agencies, and industry contributors. The database is divided into key collections:

- **Substance**: Chemical samples from data providers.

- **Compound**: Unique chemical structures derived from the substance records.

- **BioAssay**: Experimental data on biological activities of compounds.

- **Protein and gene**: Links chemicals to molecular targets.

- **Pathway**: Connects compounds to biological pathways.

- **Cell line and taxonomy**: Describe biological systems used in studies.

- **Patent**: Extracts chemical information from patent literature.

PubChem supports structure searches, bioactivity exploration, and data downloads, making it a vital tool for drug discovery, toxicology, and biomedical research [74].
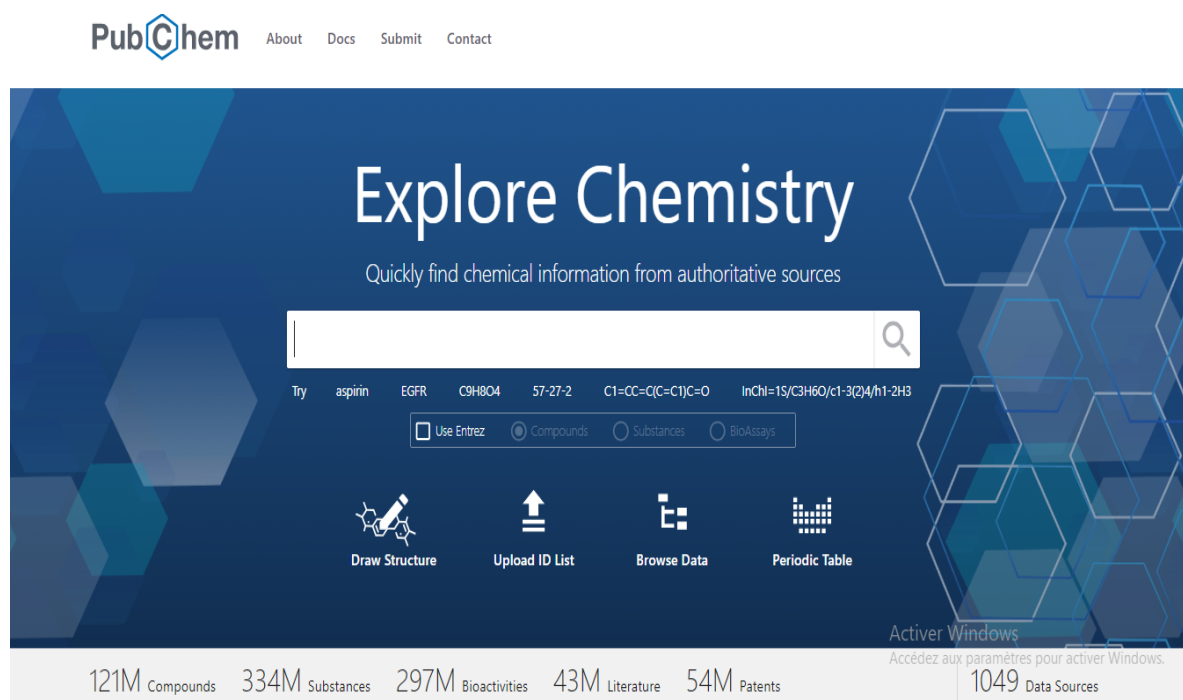
FIGURE 11: Recent screenshot of the PubChem database homepage, accessed on May 10, 2025

1.3. Pre-ADMET

PreADMET v2.0 is a freely accessible web-based server designed to offer rapid and preliminary predictions of key pharmacokinetic and toxicological properties of small molecules (figure 12). It assists researchers in the early stages of drug discovery by estimating essential ADMET characteristics Absorption, Distribution, Metabolism, Excretion, and Toxicity which are critical for assessing the drug-likeness and safety profile of candidate compounds before experimental testing.

The server supports input in multiple formats, including SMILES strings and molecular structure files (e.g., MOL or SDF), and provides a user-friendly interface for structure submission and property analysis. PreADMET utilizes a variety of predictive models based on quantitative structure–activity relationships (QSARs) and curated experimental data [75].
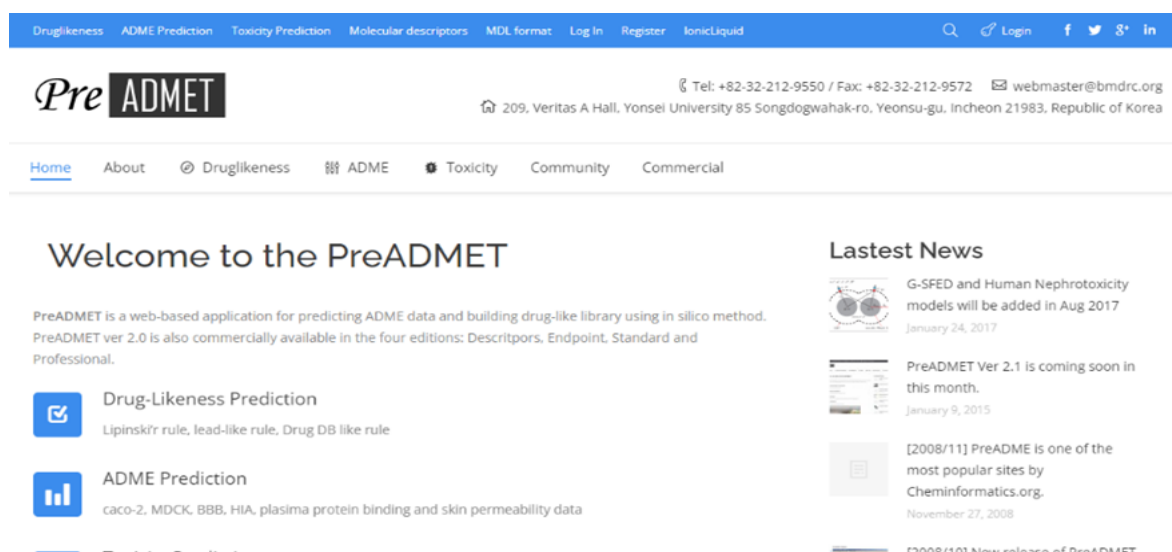
FIGURE 12: Screenshot of the PreADMET server homepage, accessed on May 10, 2025.

2. Software's and programs

2.1. AutoDock Tools

AutoDock Tools v1.5.7 (ADT) is a graphical interface designed to set up and run AutoDock simulations. It offers a free, open-source platform that enables researchers to perform molecular docking with accuracy, helping to predict how small molecules bind within the active sites of target receptors (Figure 13) [76].
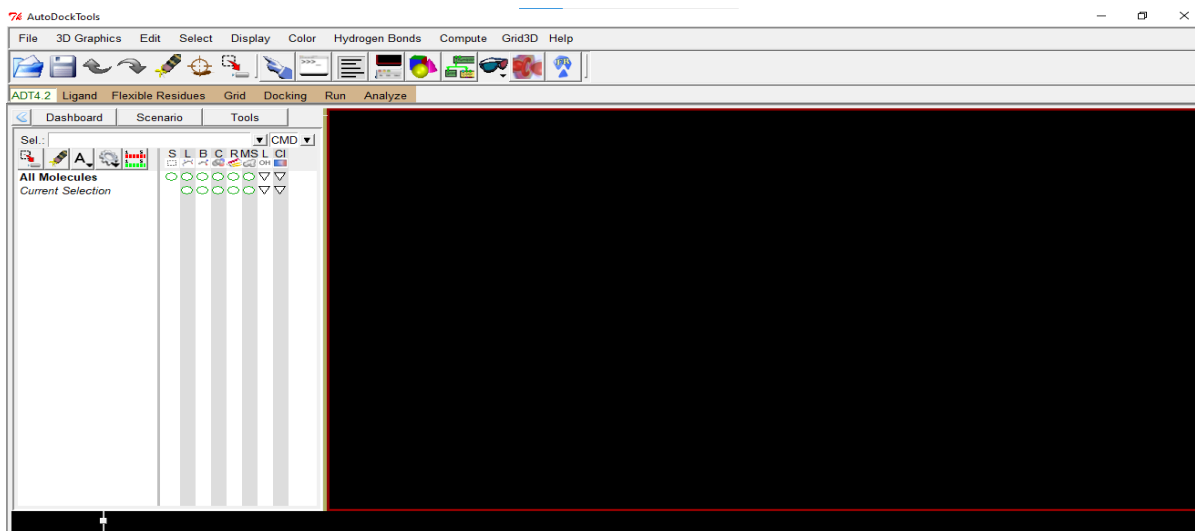
FIGURE 13: AutoDock Tools graphical user interface for preparing receptor and ligand files for molecular docking.

2.2. AutoDock Vina

AutoDock Vina (ADV) is a widely utilized open-source molecular docking program designed for precise prediction of protein-ligand interactions. It employs a hybrid search algorithm that integrates genetic algorithms with a scoring function based on empirical binding affinity data. This approach enables ADV to efficiently explore ligand conformational space within a protein's binding site, identify the most energetically favorable binding modes, and assess binding affinities [77].

2.3. Discovery studio visualizer

Discovery studio visualizer (DSV) provides a suite of tools for creating graphical representations of molecular structures and simulation results. Its visualization features enable researchers to analyze and communicate findings from molecular simulations, docking studies, and other molecular investigations. This protocol offers guidelines for displaying molecular structures in 3D, highlighting key interactions between proteins and ligands such as hydrogen bonding and hydrophobic interactions which influence complex stability and binding affinity. Additional visualization capabilities include electrostatic potential mapping, surface and volume rendering, and complex visualization. Users can customize these visualizations by adjusting settings like color, transparency, and labels (Figure 14) [78].
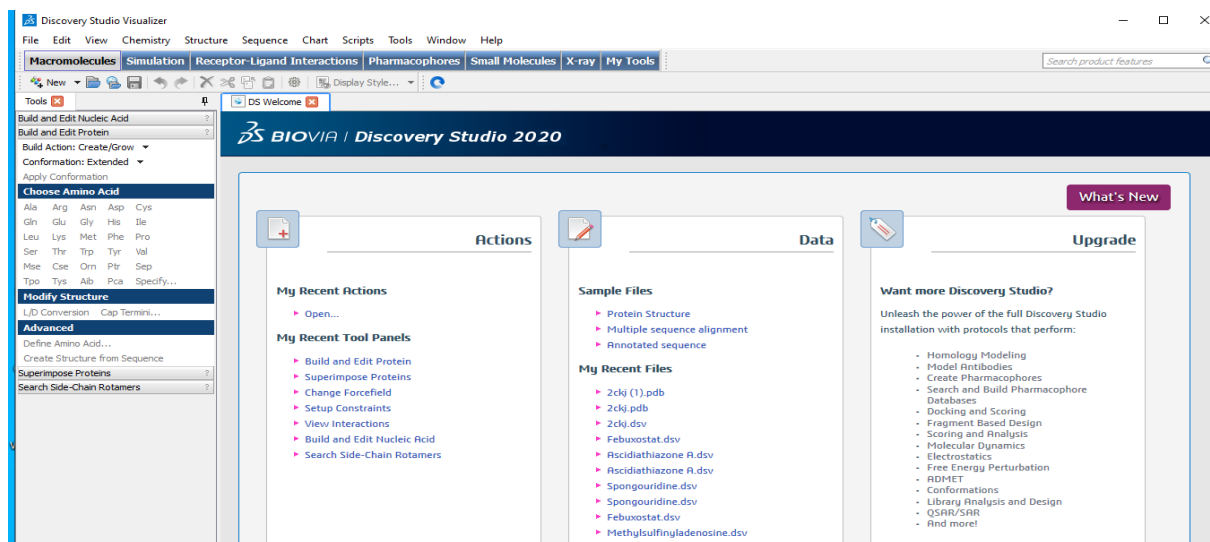
FIGURE 14: The primary interface of the DSV software.

3. Absorption, Distribution, Metabolism and Toxicity

Absorption, Distribution, Metabolism, and Toxicity (ADMT) are fundamental pharmacokinetic properties that play a vital role in the drug discovery and development process. These parameters collectively describe how a compound is absorbed into the body, how it is distributed among various tissues and organs, how it undergoes metabolic transformation, and its potential to cause toxic effects. Evaluating these characteristics is essential for assessing a drug's safety, efficacy, and overall suitability before advancing to clinical trials. Compounds with unfavorable ADMT profiles often fail during preclinical or clinical stages due to issues such as low bioavailability or adverse toxicity. In recent years, computational and *in silico* approaches have become increasingly important for early-stage prediction of ADMT profiles, allowing researchers to filter out suboptimal candidates before costly experimental procedures **[79]**.

In this study, we employed the PreADMET v2.0 web server. This server facilitated a comparative analysis of our target compounds against Allopurinol, which was used as the reference drug. It is important to note that the excretion parameter was excluded from our evaluation due to a lack of reliable predictive data for the specific compounds analyzed. The selected ADMT parameters used in our assessment are summarized in table 2.

TABLE 2: Parameters used in the ADMT study.

Parameters	Description	Standards	Reference
Absorption			
Caco-2 cell permeability (nm/sec)	Used to assess the intestinal permeability of a molecule, i.e. its ability to pass through the intestinal wall.	> 20 (best)	**[80]**
Human intestinal absorption (HIA %)		between (80-100) % are best	**[81]**
P-gp inhibition	P-glycoprotein (P-gp) protects cells from toxins and xenobiotics.	Molecules should not be inhibitor	**[82]**
Distribution			
Blood-brain barrier penetration (BBB) (C.brain/C.blood)	Is a physical barrier, which tightly controls exchanges between the blood and the cerebral compartment.	> 2 cross the blood-brain barrier easily	**[83]**
MDCK cell permeability (nm/sec)	MDCK cells are used to study the distribution of xenobiotics.	Bigger (better)	**[84]**
Plasma protein binding (%) (PPB)	To assess binding to the main plasma proteins, namely albumin, alpha1-glycoprotein, lipoproteins and globulins.	Lower (better)	**[85]**
Metabolism			
Inhibition of cytochrome P450 3A4	Assess the metabolism of 90% of xenobiotics.	Harmful effect (Inhibitor) Safe (Substrate)	**[86]**
Substrate of cytochrome P450 3A4			
Toxicity			
Ames test	The Ames test is used as a risk test to determine the mutagenic effects of xenobiotics.	Non-mutagen	**[87]**
Carcinogenicity Mouse / rat	Assessing the carcinogenic potential of xenobiotics.	Negative	**[88]**
HERG_inhibition	To assess the inhibition of the potassium channel in the heart (responsible for beating).	Negative	**[89]**

4.   Molecular docking

Molecular docking is a computational technique used in drug discovery and biochemistry to predict how small molecules (ligands) interact with a target protein or enzyme (receptors). It helps researchers understand the binding affinity and orientation of a ligand within a receptor's active site (figure 15), which is crucial for designing effective drugs **[90]**.

2CKJ   Ligand   2CKJ+ligand
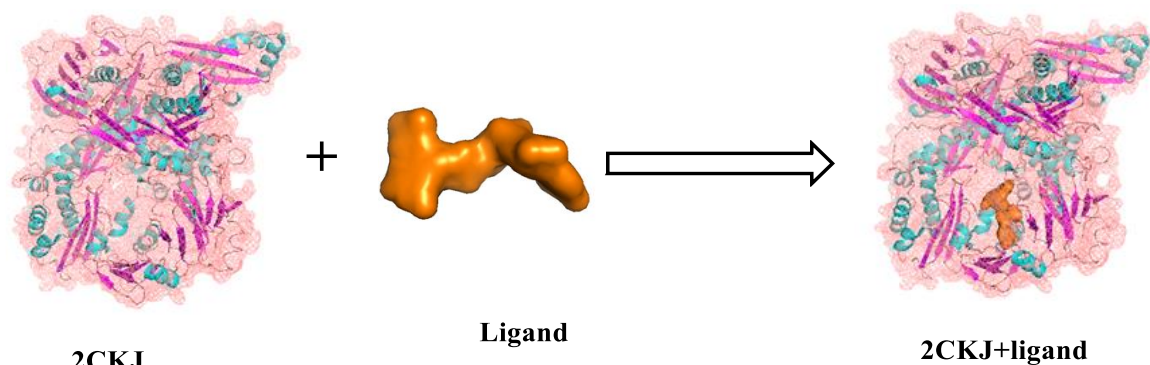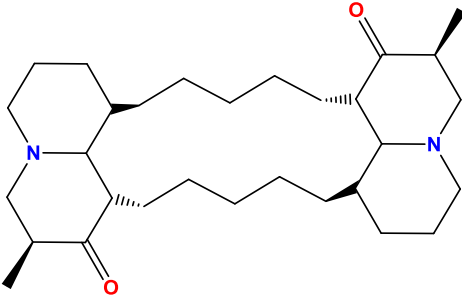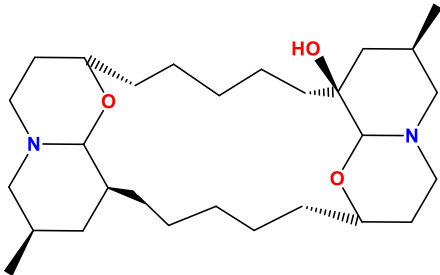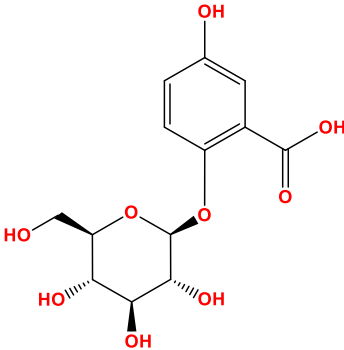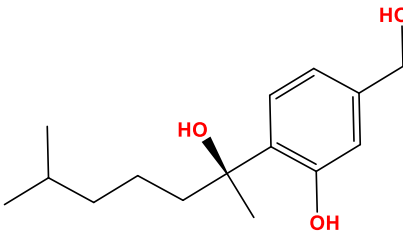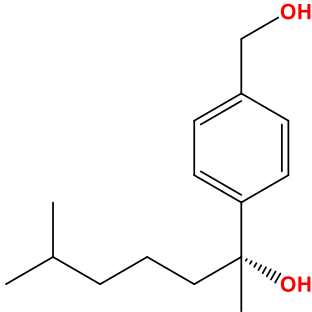
FIGURE 15: Schematic showing the stages of the docking process.

In this study, molecular docking (MD) were conducted to evaluate the inhibitory potential of five marine-derived metabolites against HXO. The selected compounds (table 3) included two alkaloids: mol1 (Petrosin) and mol2 (Xestospongin D); one phenolic acid: mol3 (Gentisic acid); and two sesquiterpenoids: mol4 (Sydonol) and mol5 (Aspergiterpenoid A).

The molecules were retrieved from the PubChem database in SDF format, converted to PDB format using DSV, and further transformed into PDBQT format using ADT for docking preparation. The aim was to estimate binding affinities and identify key molecular interactions contributing to complex formation with HXO.

The crystal structure of HXO (PDB ID: 2CKJ) was retrieved from the PDB. This structure includes a polypeptide chain and five heteroatoms: FAD, an iron-sulfur cluster (FES), glycerol (GOL), acetic acid (ACY), and a phosphate ion (PO_4). Notably, no substrate or inhibitor was present in the enzyme's active site. Allopurinol was employed as a positive control to validate the MD protocol for this target. System validation was essential to improve ligand enrichment, a critical aspect of the docking workflow.

TABLE 3: Used compounds 2D structures and their major chemical properties.

Inhibitors	Sponge	2D structure	Reference
Petrosin **(Mol1)** MF: $C_{30}H_{50}N_2O_2$ MW: 470.7 g/mol MC: Quinolizidine alkaloid PubChem ID : 3009290	*Oceanapia sp*		[54]
Xestospongin D **(Mol2)** MF: $C_{28}H_{50}N_2O_3$ MW: 462.7 g/mol MC: Quinolizidine alkaloid PubChem ID : 9847216			
Gentisic acid **(Mol3)** MF: $C_{13}H_{16}O_9$ MW: 316.26 g/mol MC: Phenolic acid PubChem ID : 49859721	*Hemimycale columella*		[64]
(S)-(+)-Sydonol **(Mol4)** MF: $C_{15}H_{24}O_3$ MW: 252.35 g/mol MC: Sesquiterpenoid PubChem ID : 25112062	*Xestospongia testudinaria*		[72]
Aspergiterpenoid A **(Mol5)** MF: $C_{15}H_{24}O_2$ MW: 236.35 g/mol MC: Sesquiterpenoid PubChem ID : 156580533			

MF: Molecular formula   **MW**: Molecular weight   **MC**: Metabolite class

To assess the accuracy of the docking results, a self-docking approach was used, in which the natural substrate, xanthine, was docked into the enzyme's active site. This step confirmed the reliability of the docking methodology.

In this study, MD was carried out as a flexible docking approach, allowing full flexibility of the ligand and partial flexibility of the enzyme's catalytic site. Protein preparation consisted of three main steps:

- **Removal of unnecessary molecules***:* In this step, all non-essential components were removed from the enzyme structure, including water molecules, heteroatoms, ligands, and co-ligands except those required in the active site.

- **Addition of polar hydrogens and partial charges**: Polar hydrogens and partial atomic charges were added to the protein structure using the ADT software, which is essential for accurate molecular docking.

- **Grid Box (GB) setup**: The grid box was defined using ADT by specifying the x, y, and z coordinates of its centre (x = 4.553, y = 77.579, z = 118.879) and its dimensions (size: x = 40, y = 40, z = 40). Once the grid box was configured **[91]**, MD was carried out using the ADV program.

RESULTS AND DISCUSSION

1. Absorption, Distribution, Metabolism and Toxicity

The predicted ADMT parameters for all compounds are summarized in table 4. The results show that Mol1, Mol5, and the control compound exhibit low Caco-2 cell permeability (ranging from 0.78 to 16.50 nm/sec), suggesting limited ability to cross-intestinal epithelial barriers. In contrast, Mol2, Mol3, and Mol4 display higher permeability values (ranging from 28.80 to 55.67 nm/sec), indicating better potential for membrane penetration. Despite differences in permeability, except Mol5, all compounds demonstrate high-predicted human intestinal absorption, ranging from 85 % to 97 %, surpassing the absorption rate of the control drug, allopurinol.

Regarding P-glycoprotein (P-gp) interactions, Mol1, Mol2, Mol5, and the control compound are predicted to be neither inhibitors nor substrates of P-gp. This suggests they are less likely to be actively effluxed from cells, which may contribute to higher intracellular concentrations and improved bioavailability favorable characteristics for oral administration. In contrast, Mol3 and Mol4 are predicted to act as P-gp inhibitors, indicating a potential to interfere with the efflux of other compounds. This interaction may influence the pharmacokinetics of co-administered drugs and increase the risk of drug–drug interactions.

The predicted distribution profiles of the selected compounds reveal varying capacities to penetrate the blood-brain barrier (BBB). Approximately half of the compounds exhibit limited BBB permeability, with values ranging from 0.21 to 1.78, indicating potential challenges in accessing the central nervous system. In contrast, Mol2, Mol3, and Mol4 demonstrate high BBB permeability scores (ranging from 4.43 to 8.57), suggesting that these compounds may have the potential to exert neurological activity or central nervous system effects.

In terms of MDCK cell permeability which serves as a model for predicting tissue distribution Mol1, Mol2, and the control compound exhibit high permeability values (>19 nm/s), indicating strong potential for effective distribution into body tissues.

Mol3 demonstrates moderate permeability (10.38 nm/s), suggesting sufficient, though less efficient, tissue penetration. In contrast, Mol4 and Mol5 show low MDCK permeability (<1 nm/s), indicating poor tissue absorption. This limited permeability may hinder their systemic bioavailability and could necessitate alternative administration strategies or formulation enhancements to improve therapeutic delivery.

The predicted plasma protein binding (PPB) values indicate that all compounds, except Mol5, exhibit high binding affinity to plasma proteins such as albumin. This strong binding can limit the free (pharmacologically active) concentration of the drug in the bloodstream, potentially necessitating higher doses to achieve effective levels at the target site. However, increasing the dose may elevate the risk of side effects or toxicity, particularly if albumin-binding sites become saturated. Once saturation occurs, excess drug remains unbound, which can significantly increase the risk of adverse effects. Therefore, understanding PPB is critical for optimizing dosage and ensuring therapeutic safety. In contrast, Mol5 shows low plasma protein binding, suggesting it remains largely unbound in circulation. This characteristic may enhance its immediate bioavailability and enable lower dosing to achieve therapeutic efficacy, thereby reducing the potential for dose-related toxicity.

The cytochrome P450 metabolism predictions for the five marine-derived metabolites provide valuable insights into their potential pharmacokinetic behavior and associated drug interaction risks, particularly in relation to the major isoenzymes CYP2D6 and CYP3A4. Among the compounds, Mol3 and Mol4 are notable as the only predicted inhibitors of CYP2D6, indicating a potential to interfere with the metabolism of co-administered drugs processed by this enzyme. Furthermore, both Mol3 and Mol4 are predicted to be CYP2D6 substrates, suggesting that they may themselves be metabolized via this pathway implying a potential risk of self-inhibition. In contrast, Mol1, Mol2, Mol5, and the control compound showed no interaction with CYP2D6, indicating a reduced metabolic liability through this isoform.

Regarding CYP3A4, all compounds except Mol5 are predicted to act as inhibitors. Notably, Mol4 is predicted to be a full substrate, while Mol1, Mol3, and Mol5 are identified as weak substrates, implying a potential risk of self-inhibition. The control compound is also a CYP3A4 inhibitor but is not a substrate, suggesting it may exhibit metabolic stability while still interfering with the metabolism of other drugs. In contrast, Mol5 presents a more favorable metabolic profile, acting as a weak substrate of CYP3A4 without inhibitory effects, thereby minimizing the risk of enzyme-mediated interactions.

Overall, Mol5 appears to be a safer candidate in terms of CYP3A4 and CYP2D6 related interactions, whereas the remaining compounds particularly Mol3 and Mol4 warrant further investigation due to their potential inhibitory activity and dual roles as substrates.

The toxicity prediction revealed highly encouraging results across all tested marine-derived secondary metabolites (Table 1). None of the selected compounds demonstrated carcinogenic effects in standard rodent models (mouse and rat), indicating a low potential for long-term cancer risk. Additionally, predictions for HERG channel inhibition a critical marker for cardiac safety showed low risk for all compounds. Notably, the control compound was the only one found to possess mutagenic potential, carcinogenic effects, and a higher risk for HERG inhibition, which may explain its known secondary effects, including possible cardiotoxicity and long-term safety concerns. Together, these results suggest a favorable safety profile for the marine-derived compounds, supporting their continued development as promising therapeutic candidates.

Excretion parameters, including renal and biliary clearance, were not assessed in this study due to the limited or insufficient data available for the selected marine-derived compounds. Reliable prediction of excretion requires comprehensive physicochemical and metabolic information, such as metabolic stability and specific transporter interactions. However, given the novelty of these compounds, especially those derived from marine sources, current

computational tools offer poor or inconclusive predictions in this domain. As a result, excretion profiling was excluded from the pharmacokinetic analysis to avoid speculative or unreliable conclusions. Future experimental studies will be necessary to accurately determine the excretory behavior of these compounds.

TABLE 4: ADMT parameters of the selected compounds.

Pharmacokinetics	Mol1	Mol2	Mol3	Mol4	Mol5	Control
Absorption						
Caco-2 cell permeability (nm/sec) > 20	16.50	28.80	37.17	55.67	0.78	10.26
Human intestinal absorption (HIA %) 80 to 100 %	86.11	91.60	95.89	97.63	15.85	85.70
P-glyco protein inhibition should not inhibit a substrate of it indicates high levels absorption	Non	Non	Inhibitor	Inhibitor	Non	Non
Distribution						
Blood-brain barrier penetration (C.brain/C.blood) (BBB) > 2 cross the blood–brain barrier easily	1.78	4.43	8.57	6.59	0.21	0.22
MDCK cell permeability (nm/sec) Low (< 1 nm/s), moderate (1-10 nm/s), and high (>10 nm/s)	19.14	29.08	10.38	0.044	0.61	29.95
Plasma protein binding (%) (PPB) 80 to 100 % is considered high, 50 to 80 % (moderate), < 50 % (low)	100	93.90	75.61	80.91	33.19	91.36
Metabolism						
Cytochrome P450 2D6 inhibition	Non	Non	Inhibitor	Inhibitor	Non	Non
Cytochrome P450 2D6 substrate	Non	Non	Substrate	Substrate	Non	Non
Cytochrome P450 3A4 inhibition	Inhibitor	Inhibitor	Inhibitor	Inhibitor	Non	Inhibitor
Cytochrome P450 3A4 substrate	Weakly	Non	Weakly	Substrate	Weakly	Non
Toxicity						
Ames test	Non-mutagen	Non-mutagen	Non-mutagen	Non-mutagen	Mutagen	Mutagen
Carcinogenicity (Mouse)	Negative	Negative	Negative	Negative	Negative	Positive
Carcinogenicity (Rat)	Negative	Negative	Negative	Negative	Negative	Negative
HERG_inhibition	low_risk	low_risk	low_risk	low_risk	low_risk	Medium risk

HERG: Human ether related gene channel **MDCK:** Mandin Darby Canine Kidney **Caco-2:** Human colorectal carcinoma

🟩 **Safe**   🟧 **Medium risk**   🟥 **Unsafe**

2. Molecular docking

The analysis of the MD results for our five compounds shows significant findings based on the lowest binding energy, which ranges between -7.2 and -11.5 kcal/mol. Mol1 was the best inhibitor among the other tested alkaloids, with a value of -11.5 kcal/mol compared to the control (-5.9 kcal/mol). All results are summarized in table 5.

TABLE 5: Analysis of the MD results.

Ligand	Energy (Kcal/mol)	Active site residues	Hydrophobic Interactions	Hydrogen bond (Å)	Fav /Unfav bond
Xanthine (Substrate)	**-6.2**	Glu263, Ala346 Val259, Gly260 Asn261, Thr262 Gly350, Thr354	π-Alkyl, π-Anion	Val259 (1.86) Gly260 (2.20) Asn261 (1.96) Thr262 (2.57) Gly350 (2.73) Thr354 (2.20)	8/0
Allopurinol (Control)	**-5.9**	Ala346, Val259, Gly260, Asn261	π-Alkyl	Gly260 (2.20) Asn261 (1.96)	4/0
Petrosin (mol1)	**-11.5**	Lys395, Val259 Leu257, Ile353, Thr396	Alkyl	Leu257 (2.27) Thr396 (2.13) Thr396 (2.34)	6/0
Xestospongin D (Mol2)	**-8.8**	Glu263, Thr262 Ala432	-	Glu263 (2.11) Thr262 (2.58) Glu263 (2.85) Ala432 (2.61)	5/0
Gentisic acid (mol3)	**-7.3**	Leu257, Val259 Gly260, Asn261 Glu263, Gly350 Ile353	π-Alkyl	Val259 (1.92) Asn261 (2.76) Glu263 (2.77) Leu257 (2.60) Gly350 (2.70)	8/2
Sydonol (mol4)	**-7.3**	Leu257, Val259 Pro281, Leu287 Ala301, Gly350 Ile353, Thr354	π –alkyl Alkyl	Gly350 (2.29) Thr354 (2.55)	10/0
Aspergiterpenoid A (mol5)	**-7.2**	Leu257, Val259 Gly260, Thr262 Pro281, Leu287 Ala301, Ile353	π –alkyl Alkyl	Gly260 (2.77)	8/2

Å : Angstrom   **Fav /Unfav:** Favorable/Unfavorable

Xanthine oxidase is a molybdo-flavin oxidoreductase **[92]** whose cofactor is NAD or FAD, **[93]**. It is primarily found in the liver and intestine **[94]**. HXO plays a key role in purine

metabolism **[95]** by promoting their oxidation into UA **[96]**. Its hyperactivity leads to hyperuricemia and gout **[97]**.

The crystal structure of HXO was analyzed in the absence of any bound substrate or inhibitor, as previously noted. To validate the docking protocol, MD was performed using both xanthine (the natural substrate) and allopurinol (a known competitive inhibitor). The results highlight key differences in their binding interactions, which are consistent with their structural distinctions. Structurally, xanthine is a purine derivative featuring two carbonyl groups at positions 2 and 6 of the purine ring. In contrast, allopurinol is a structural isomer of hypoxanthine, possessing a pyrazolo[3,4-d]pyrimidine scaffold with a single carbonyl group at position 4. This shift in ring configuration alters the electronic distribution and hydrogen bonding potential, directly influencing their binding modes within the active site of HXO.

The docking results provide insight into the distinct binding behaviors of xanthine and allopurinol within the active site of HXO, directly reflecting their structural differences.

Xanthine, the natural substrate, exhibited a higher number of hydrogen bonds (six in total) distributed between both its pyrimidine and imidazole rings (figure 16), which reflects its optimized fit and recognition by the enzyme. These interactions include key residues such as Gly260, Asn261, Val259, Gly350, Thr354, and Thr262, stabilizing the substrate through extensive polar contacts.

In contrast, **allopurinol**, despite being an effective inhibitor, formed only two hydrogen bonds and two hydrophobic interactions. Its modified pyrazolo[3,4-d]pyrimidine ring lacks the same number of hydrogen-bond donors/acceptors as xanthine and adopts a slightly different orientation in the binding pocket (figure 16). However, its favorable interactions especially with Gly260, Asn261, and Ala346 allow it to mimic xanthine's position and effectively block substrate access. This supports allopurinol's mechanism of action as a competitive inhibitor that is further metabolized into oxypurinol, a more potent, long-lasting form. Overall, the greater

hydrogen bonding capacity of xanthine correlates with its role as a substrate, whereas allopurinol's lower but targeted binding interactions enable effective active site inhibition. These differences are critical for rational drug design targeting HXO and provide a molecular basis for allopurinol's inhibitory action.

Xanthine   **Allopurinol**

| | Conventional Hydrogen Bond | | π- anion | | π-alkyl |
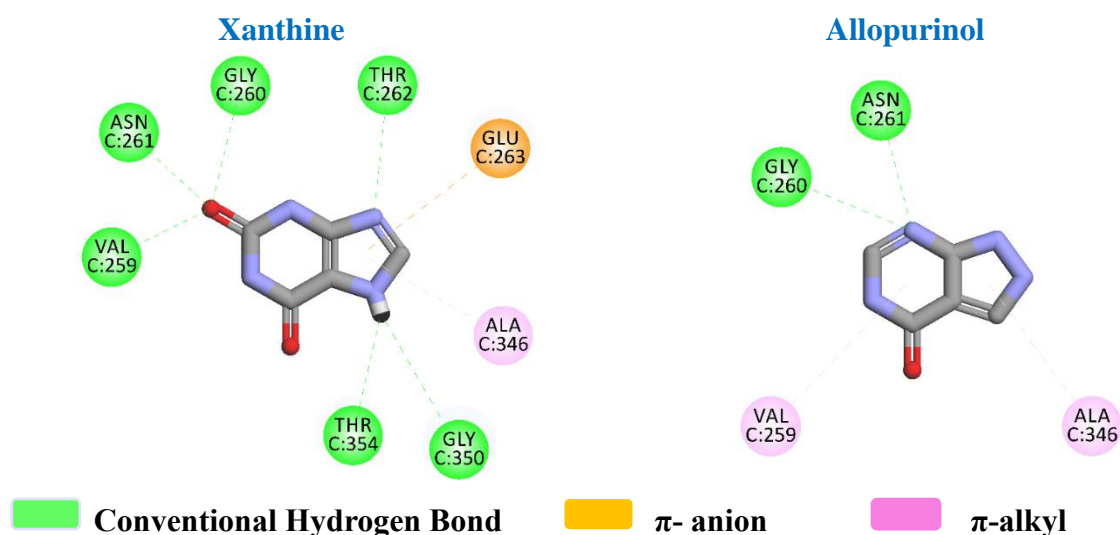
FIGURE 16: 2D interaction diagrams illustrating the molecular docking of xanthine (substrate) and allopurinol (reference inhibitor) with HXO.

.

Mol1, corresponding to Petrosin, is a bisquinolizidine alkaloid exhibiting a complex 3D knotted structure (figure 17). Its molecular architecture includes two amine groups, two hydroxyl groups, and a long, branched carbon chain. It is classified as a polycyclic aliphatic compound (figure 17).

Among the ligands evaluated for their binding affinity to HXO, Mol1 demonstrates the lowest binding energy (table 5), outperforming both the control compound and the natural substrate. This low binding energy indicates a highly stable complex with the enzyme and suggests a strong binding affinity, making Mol1 a promising candidate for the development of HXO inhibitors. At the molecular level, Mol1 interacts with HXO through three key conventional hydrogen bonds involving residues Leu257 and Thr396, located at the entrance of the enzyme's active site. Additionally, Mol1 forms three significant hydrophobic interactions with residues

Lys395, Ile353, and Val259. These interactions collectively allow Mol1 to block access to the active site, thereby preventing substrate entry (figure 17).
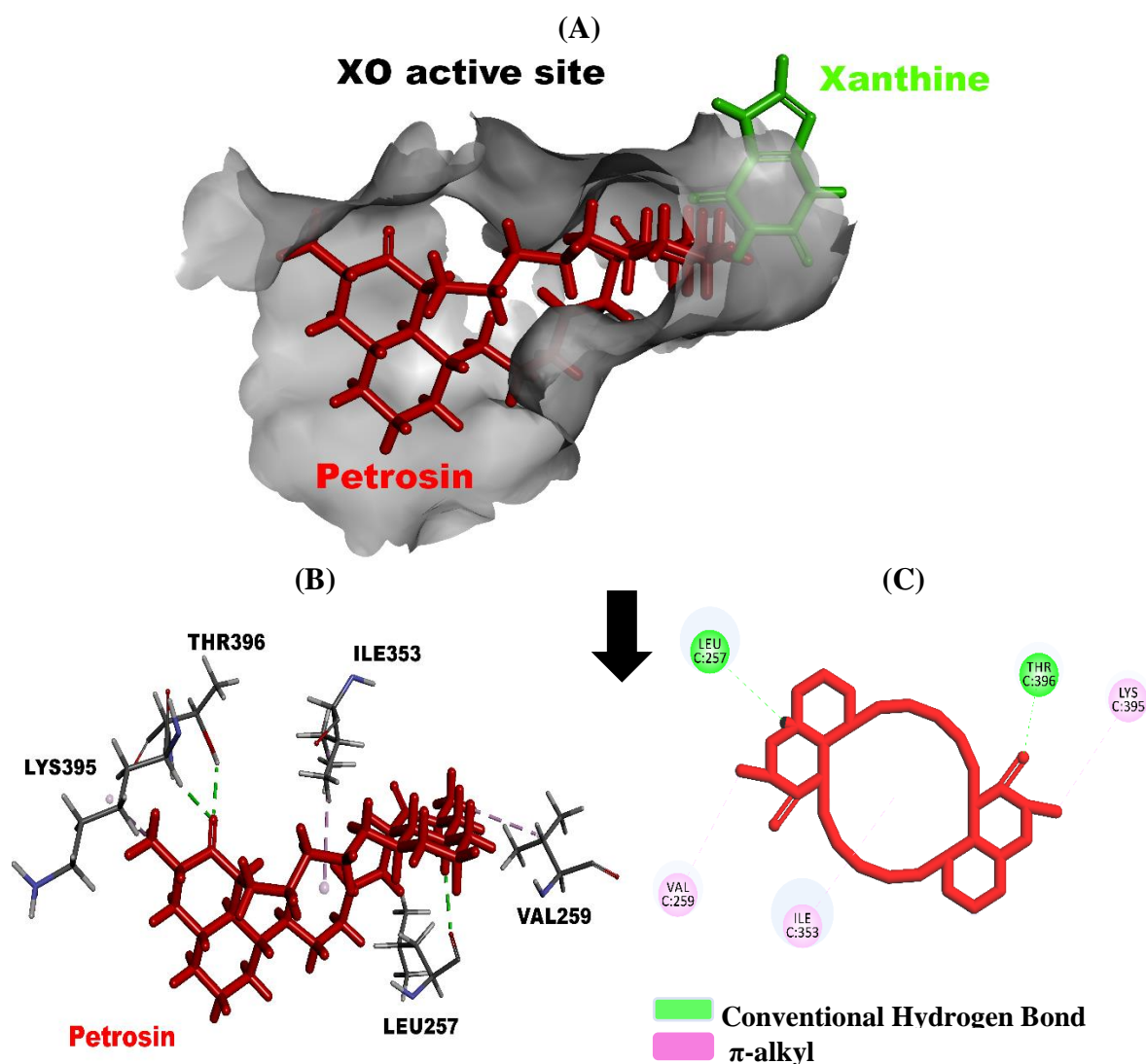
FIGURE 17: Molecular docking analysis of Petrosin with HXO.
(A) Surface representation of HXO showing Petrosin occupying the active site, effectively blocking substrate access. **(B)** 3D binding pose of Petrosin within the HXO active site, highlighting key interacting residues involved in hydrogen bonding and hydrophobic interactions. **(C)** 2D interaction diagram, illustrating conventional hydrogen bonds and hydrophobic contacts between Petrosin and active site residues.

Mol2, corresponding to Xestospongin D, is a polycyclic ether alkaloid featuring a rigid pentacyclic core (figure 18). Its structure includes two oxygen atoms forming ether linkages, two nitrogen atoms incorporated into the polycyclic framework, and a terminal hydroxyl group, contributing to both its conformational rigidity and capacity for polar interactions. It is classified as a polycyclic aliphatic amine ether (figure 18). Mol2 displayed a notably low

binding energy (table 5), comparable to or slightly higher than that of Mol1, suggesting a strong and stable interaction with the enzyme. However, unlike Mol1, which occupies the entrance of the active site and physically blocks substrate access, Mol2 appears to interact via a distinct binding mode**.**

At the molecular level, Mol2 forms multiple carbon hydrogen bonds involving residues such as Glu263**,** Ala432, and Thr262, positioned deeper within or adjacent to the allosteric pocket of HXO. Importantly, the binding of Mol2 does not directly occlude the catalytic center, but instead induces subtle conformational changes that may alter the geometry or accessibility of the active site. This mechanism of action is consistent with non-competitive or allosteric inhibition, setting Mol2 apart from Mol1, which acts via direct competitive inhibition. Consequently, Mol2 represents a structurally and mechanistically distinct scaffold with potential for development as a novel class of HXO inhibitors**.**

(A)   **(B)**

FIGURE 18: Molecular docking analysis of Xestospongin D with HXO.
(A) 3D best pose within the binding pocket, highlighting key interacting residues.
(B) 2D interaction diagram.

Mol3, identified as Gentisic acid, is a phenolic acid composed of a benzene ring substituted with two hydroxyl groups and a carboxylic acid moiety (figure 19). This small, planar aromatic compound is well-suited for polar interactions within enzyme binding sites. Mol3 exhibited a binding energy moderately higher than that of Mol1 (Petrosin) and Mol2 (Xestospongin D),

placing it third in terms of predicted affinity (table 5). Mol3 binds within the active site of HXO and forms five conventional hydrogen bonds with key residues: Val259, Asn261, Glu263, Leu257, and Gly350. These polar interactions are complemented by π-alkyl hydrophobic contacts, further stabilizing the ligand-enzyme complex. However, Mol3 also exhibited two unfavorable interactions, which may slightly compromise its overall binding efficiency. Nonetheless, its binding mode suggests a competitive inhibition mechanism, directly interfering with substrate access to the catalytic center.
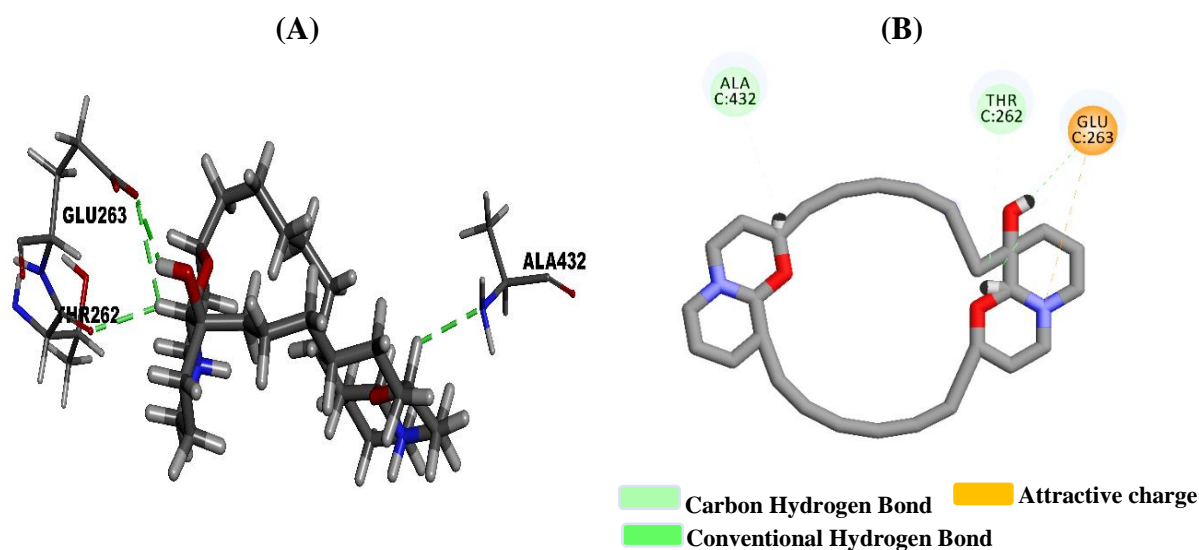

FIGURE 19: Molecular docking analysis of Gentisic acid with HXO.
(A) 3D best pose within the binding pocket, highlighting key interacting residues.
(B) 2D interaction diagram

Mol4, corresponding to Sydonol, is a sesquiterpenoid characterized by a three hydroxyl groups (figure 20). This structure combines polar functional groups with an extended hydrophobic side chain, enabling diverse interactions within the enzyme's binding pocket. Mol4, like Mol3, binds within the active site of HXO and shows a binding energy of similar magnitude, indicating moderate but favorable affinity (table 5). It forms two conventional hydrogen bonds with Gly350 and Thr354, and engages in a total of nine hydrophobic interactions, the majority of which are of the alkyl type, along with some π-alkyl contacts. This

dense network of hydrophobic interactions likely represents the primary mode of binding for Mol4, compensating for its limited polar contacts. Notably, Mol4 exhibited no unfavorable interactions, contributing to its overall stability within the active site. These features support a competitive inhibition mechanism, and highlight Mol4's potential as a structurally distinct, hydrophobically driven inhibitor of HXO.

(A)   **(B)**

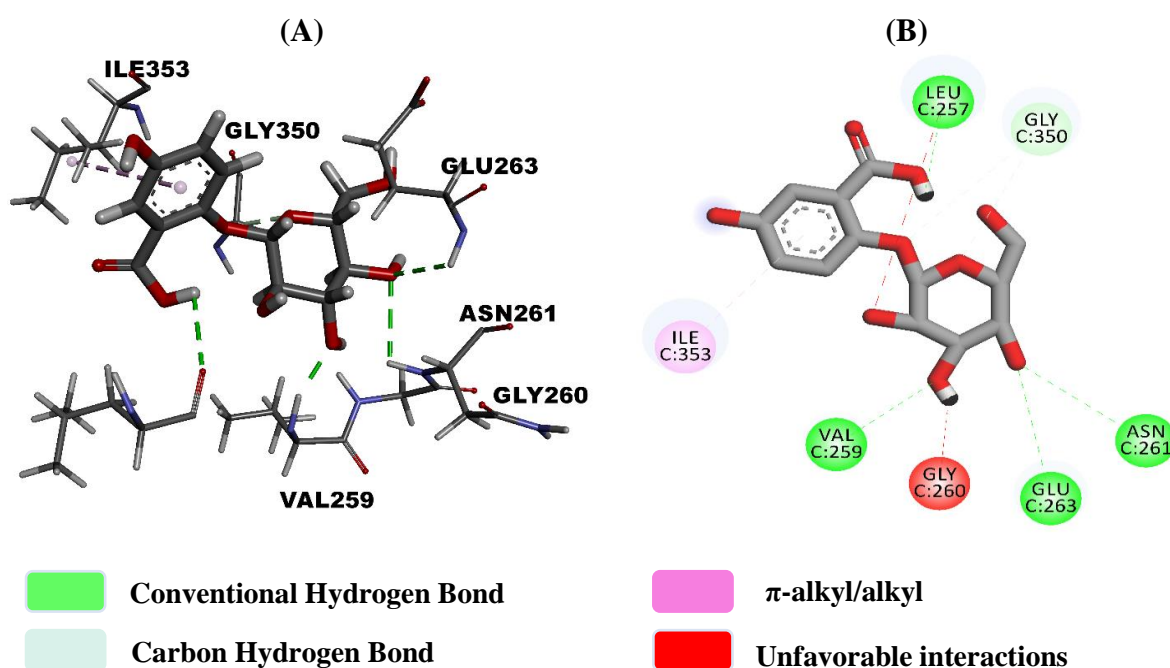| Conventional Hydrogen Bond	π-alkyl/alkyl
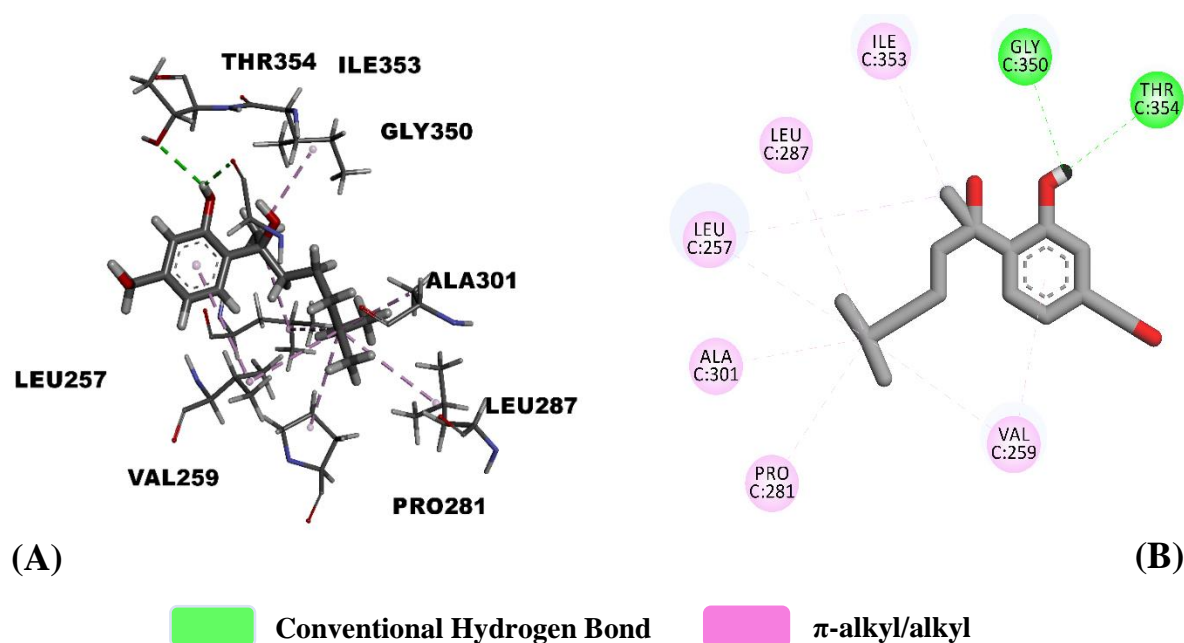
FIGURE 20: Molecular docking analysis of Sydonol with HXO.
(A) 3D best pose within the binding pocket, highlighting key interacting residues.
(B) 2D interaction diagram.

Mol5, corresponding to Aspergiterpenoid A, also classified as a sesquiterpenoid, shares structural and mechanistic similarities with Mol4, particularly in terms of binding affinity and complex stability with HXO (table 5). Its sesquiterpenoid scaffold features a compact hydrophobic framework capable of occupying the enzyme's active site while supporting limited polar interactions (figure 21). Mol5 was found to bind within the active site of HXO and exhibited a binding energy comparable to that of Mol4, suggesting a stable and energetically favorable interaction. Mol5 formed a single conventional hydrogen bond with Gly260, reflecting a minimal polar contact profile. This interaction is complemented by a substantial network of seven hydrophobic interactions, primarily of the alkyl type, along with one π-alkyl

interaction, indicating that hydrophobic interactions constitute the dominant mode of binding. However, Mol5 also exhibited two unfavorable interactions, which may slightly affect the overall binding efficiency. Despite this, the compound maintains a stable position within the catalytic site, supporting a competitive inhibition mechanism. These findings highlight Mol5 as a structurally distinct sesquiterpenoid with moderate affinity and a primarily hydrophobic interaction profile, reinforcing its potential as a candidate for HXO inhibition.

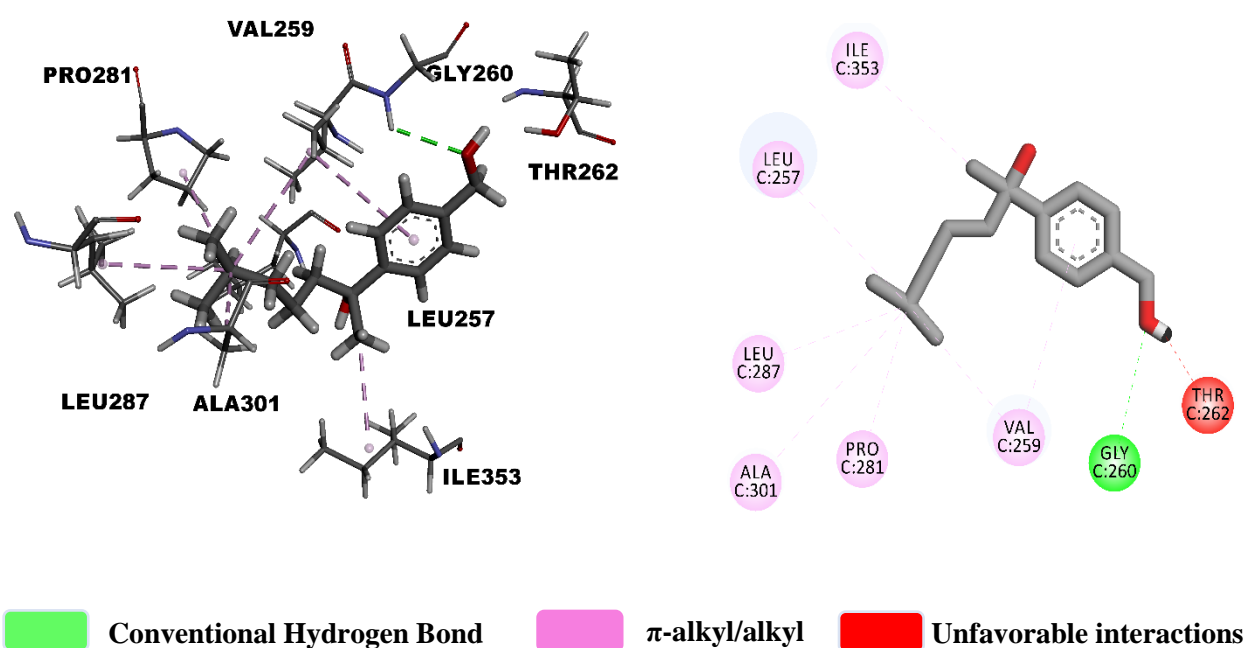| Conventional Hydrogen Bond | π-alkyl/alkyl | Unfavorable interactions |

FIGURE 21: Molecular docking analysis of Aspergiterpenoid A with HXO.
The most favorable binding conformation is illustrated in both 3D and 2D representations.

CONCLUSION AND PERSPECTIVES

In this *in silico* study, we aimed to identify marine invertebrate-derived secondary metabolites as potential inhibitors of HXO with reduced side effect profiles. A multi-step approach was implemented, encompassing literature-based compound selection, pharmacokinetic profiling (ADMT), and MD analysis to assess binding interactions and therapeutic potential. From the marine sponge *Oceanapia sp.,* two alkaloids were selected: Petrosin (Mol1) and Xestospongin D (Mol2). A phenolic acid, Gentisic acid (Mol3), was chosen from *Hemimycale columella*. Additionally, two sesquiterpenoids Sydonol (Mol4) and Aspergiterpenoid A (Mol5) were examined, both derived from a fungal strain (*Aspergillus sp.*) isolated from the sponge *Xestospongia testudinaria*.

The ADMT profiling offers valuable insights into the pharmacokinetic behavior and safety of the selected marine-derived compounds. Mol2, Mol3, and Mol4 exhibit favorable characteristics, including high intestinal absorption, strong Caco-2 cell permeability, and notable blood-brain barrier penetration, along with moderate interaction with cytochrome P450 enzymes. Mol1 and Mol5 show superior membrane permeability and minimal interaction with P-glycoprotein, which supports their potential for efficient oral bioavailability. Although Mol1 is predicted to interact with CYP3A4, the associated metabolic liabilities may be mitigated through appropriate dosing or formulation strategies. Importantly, all compounds demonstrate favorable toxicity profiles, with Mol5 standing out due to its low plasma protein binding and minimal CYP-related interaction risk. Collectively, these findings highlight the promising pharmacokinetic and safety attributes of the studied compounds as potential therapeutic agents.

Crucially, the molecular docking results highlight Mol1 and Mol2 as the most promising candidates, showing the strongest binding affinities among the tested compounds. Both molecules bind directly within the active site of HXO, establishing key interactions with catalytic residues, indicative of a competitive inhibition mechanism. Similarly, Mol3, Mol4, and Mol5 also demonstrated strong binding within the active site, reinforcing their potential as

effective inhibitors. Notably, all five selected compounds outperformed both the control and the natural substrate in terms of binding affinity, confirming their strong and stable interactions with HXO.

Taken together, the combination of favorable docking scores, active site engagement, and acceptable toxicity profiles supports the progression of these marine-derived metabolites as lead candidates for the development of novel HXO inhibitors. Comprehensive *in vitro* and *in vivo* studies will be conducted to validate these findings.

BIBLIOGRAPHIC REFERENCES

1. Nuki, G.; Simkin, P. A., A concise history of gout and hyperuricemia and their treatment. *Arthritis research & therapy* 2006**,** *8 Suppl 1* (Suppl 1), S1.

2. Galassi, F. M.; Ingaliso, L.; Papa, V.; Lorenzi, R.; Percivaldi, E.; Varotto, E., On the early uses of the word 'gout': novel evidence and a critical assessment of the published literature. *Reumatismo* 2024**,** *76* (2).

3. Sydenham, T. Complete Dictionary of Scientific Biography. https://www.encyclopedia.com/science/dictionaries-thesauruses-pictures-and-press-releases/sydenham-thomas (accessed Retrieved May 29, 2025 from Encyclopedia.com).

4. Singh, J. A., Quality of life and quality of care for patients with gout. *Current rheumatology reports* 2009**,** *11* (2), 154-60.

5. Poznyak, A. V.; Litvinova, L.; Poggio, P.; Sukhorukov, V. N.; Orekhov, A. N., Effect of glucose levels on cardiovascular risk. *Cells* 2022**,** *11* (19), 3034.

6. Abhishek, A.; Roddy, E.; Doherty, M., Gout - a guide for the general and acute physicians. *Clinical medicine (London, England)* 2017**,** *17* (1), 54-59.

7. Maquin, E. La goutte, une maladie en recrudescence: enquête à l'officine. Université de Lorraine, 2018.

8. Liu, X.; Wu, D.; Liu, J.; Li, G.; Zhang, Z.; Chen, C.; Zhang, L.; Li, J. J. F. C. X., Characterization of xanthine oxidase inhibitory activities of phenols from pickled radish with molecular simulation. 2022**,** *14*, 100343.

9. Hainer, B. L.; Matheson, E.; Wilkes, R. T., Diagnosis, treatment, and prevention of gout. *American family physician* 2014**,** *90* (12), 831-6.

10. Zeng, D.; Yin, C.; Wei, H.; Li, Y.; Yang, Y.; Nie, H.; Pan, Y.; Xu, R.; Tai, Y.; Du, J. J. B.; Pharmacotherapy, Activation of Nrf2 antioxidant signaling alleviates gout arthritis pain and inflammation. 2024**,** *170*, 115957.

11. Shejul, P. P.; Raheja, R. K.; Doshi, G. M., An Update on Potential Antidepressants Derived from Marine Natural Products. *Central nervous system agents in medicinal chemistry* 2023**,** *23* (2), 71-85.

12. Kong, Y. R.; Tay, K. C.; Su, Y. X.; Wong, C. K.; Tan, W. N.; Khaw, K. Y., Potential of Naturally Derived Alkaloids as Multi-Targeted Therapeutic Agents for Neurodegenerative Diseases. *Molecules (Basel, Switzerland)* 2021**,** *26* (3).

13. Santhiravel, S.; Dave, D.; Shahidi, F., Bioactives from marine resources as natural health products: A review. *Pharmacological reviews* 2024, 10.1124/pharmrev.124.001227.

14. Anjum, K.; Abbas, S. Q.; Shah, S. A. A.; Akhter, N.; Batool, S.; ul Hassan, S. S., Marine sponges as a drug treasure. *Biomolecules & Therapeutics* 2016**,** *24* (4), 347.

15. Choi, H. K.; Gout, B., Epidemiology, pathology, and pathogenesis. *Primer on the Rheumatic Diseases. 13th ed. New York, NY: Springer* 2008, 250-257.

16. Ahn, E. Y.; So, M. W., The pathogenesis of gout. *Journal of rheumatic diseases* 2025**,** *32* (1), 8-16.

17. Pasalic, D.; Marinkovic, N.; Feher-Turkovic, L., Uric acid as one of the important factors in multifactorial disorders–facts and controversies. *Biochemia medica* 2012**,** *22* (1), 63-75.

18. Dalbeth, N.; Merriman, T. R.; Stamp, L. K., Gout. *Lancet (London, England)* 2016**,** *388* (10055), 2039-2052.

19. Yanai, H.; Adachi, H.; Hakoshima, M.; Katsuyama, H., Molecular Biological and Clinical Understanding of the Pathophysiology and Treatments of Hyperuricemia and Its Association with Metabolic Syndrome, Cardiovascular Diseases and Chronic Kidney Disease. *International journal of molecular sciences* 2021**,** *22* (17).

20. Fathallah-Shaykh, S. A.; Cramer, M. T., Uric acid and the kidney. *Pediatric nephrology (Berlin, Germany)* 2014**,** *29* (6), 999-1008.

21. Jensen, T.; Abdelmalek, M. F.; Sullivan, S.; Nadeau, K. J.; Green, M.; Roncal, C.; Nakagawa, T.; Kuwabara, M.; Sato, Y.; Kang, D. H.; Tolan, D. R.; Sanchez-Lozada, L. G.; Rosen, H. R.; Lanaspa, M. A.; Diehl, A. M.; Johnson, R. J., Fructose and sugar: A major mediator of non-alcoholic fatty liver disease. *Journal of hepatology* 2018**,** *68* (5), 1063-1075.

22. Reyes, A. J.; Leary, W. P., Hypertension, diuretics, and uric acid. *American journal of hypertension* 2006**,** *19* (10), 1093-4.

23. Howard, S. C.; Jones, D. P.; Pui, C. H., The tumor lysis syndrome. *The New England journal of medicine* 2011**,** *364* (19), 1844-54.

24. Zhang, W.-Z., Why does hyperuricemia not necessarily induce gout? *Biomolecules* 2021**,** *11* (2), 280.

25. Duong, N. T.; Ngoc, N. T.; Thang, N. T. M.; Phuong, B. T. H.; Nga, N. T.; Tinh, N. D.; Quynh, D. H.; Ton, N. D.; Hai, N. V., Polymorphisms of ABCG2 and SLC22A12 Genes Associated with Gout Risk in Vietnamese Population. *Medicina (Kaunas, Lithuania)* 2019**,** *55* (1).

26. Wu, Z. D.; Yang, X. K.; He, Y. S.; Ni, J.; Wang, J.; Yin, K. J.; Huang, J. X.; Chen, Y.; Feng, Y. T.; Wang, P.; Pan, H. F., Environmental factors and risk of gout. *Environmental research* 2022**,** *212* (Pt C), 113377.

27. Borghi, C.; Agabiti-Rosei, E.; Johnson, R. J.; Kielstein, J. T.; Lurbe, E.; Mancia, G.; Redon, J.; Stack, A. G.; Tsioufis, K. P., Hyperuricaemia and gout in cardiovascular, metabolic and kidney disease. *European journal of internal medicine* 2020**,** *80*, 1-11.

28. Wilcox, W. R.; Khalaf, A. A., Nucleation of monosodium urate crystals. *Annals of the rheumatic diseases* 1975, *34* (4), 332-9.

29. Allen, D. J.; Milosovich, G.; Mattocks, A. M., Crystal growth of sodium acid urate. *Journal of Pharmaceutical Sciences* 1965**,** *54* (3), 383-386.

30. Gu, H.; Yu, H.; Qin, L.; Yu, H.; Song, Y.; Chen, G.; Zhao, D.; Wang, S.; Xue, W.; Wang, L.; Ai, Z.; Xu, B.; Peng, A., MSU crystal deposition contributes to inflammation and immune responses in gout remission. *Cell reports* 2023**,** *42* (10), 113139.

31. Xu, H.; Zhang, B.; Chen, Y.; Zeng, F.; Wang, W.; Chen, Z.; Cao, L.; Shi, J.; Chen, J.; Zhu, X.; Xue, Y.; He, R.; Ji, M.; Hua, Y., Type II collagen facilitates gouty arthritis by regulating MSU crystallisation and inflammatory cell recruitment. *Annals of the rheumatic diseases* 2023**,** *82* (3), 416-427.

32. Rege, J.; Shet, T.; Naik, L., Fine needle aspiration of tophi for crystal identification in problematic cases of gout. A report of two cases. *Acta cytologica* 2000**,** *44* (3), 433-6.

33. Stewart, S.; Dalbeth, N.; Vandal, A. C.; Rome, K., The first metatarsophalangeal joint in gout: a systematic review and meta-analysis. *BMC musculoskeletal disorders* 2016**,** *17*, 69.

34. Clebak, K. T.; Morrison, A.; Croad, J. R., Gout: Rapid Evidence Review. *American family physician* 2020**,** *102* (9), 533-538.

35. Yip, K.; Berman, J. J. J., What is gout? 2021**,** *326* (24), 2541-2541.

36. Neilson, J.; Bonnon, A.; Dickson, A.; Roddy, E. J. b., Gout: diagnosis and management—summary of NICE guidance. 2022**,** *378*.

37. Filippucci, E.; Cipolletta, E.; Sirotti, S.; Filippou, G. J. G., Urate,; Disease, C. D., Optimising the Use of Ultrasound in Gout: A Review from the Ground Up. 2024**,** *2* (2), 86-100.

38. Xu, Y.; Gong, H.; Zou, Y.; Mao, X. J. J. o. D. S., Antihyperuricemic activity and inhibition mechanism of xanthine oxidase inhibitory peptides derived from whey protein by virtual screening. 2024**,** *107* (4), 1877-1886.

39. Engel, B.; Just, J.; Bleckwenn, M.; Weckbecker, K., Treatment options for gout. *Deutsches Ärzteblatt International* 2017**,** *114* (13), 215.

40. Kusano, T.; Nishino, T.; Okamoto, K.; Hille, R.; Nishino, T. J. R. B., The mechanism and significance of the conversion of xanthine dehydrogenase to xanthine oxidase in mammalian secretory gland cells. 2023**,** *59*, 102573.

41. Pauff, J. M.; Zhang, J.; Bell, C. E.; Hille, R. J. J. o. B. C., Substrate orientation in xanthine oxidase: crystal structure of enzyme in reaction with 2-hydroxy-6-methylpurine. 2008**,** *283* (8), 4818-4824.

42. Pauff, J. M.; Cao, H.; Hille, R. J. J. o. b. c., Substrate orientation and catalysis at the Molybdenum site in xanthine oxidase. 2009**,** *284* (13), 8760-8767.

43. Cao, H.; Pauff, J. M.; Hille, R., Substrate orientation and catalytic specificity in the action of xanthine oxidase: the sequential hydroxylation of hypoxanthine to uric acid. *The Journal of biological chemistry* 2010**,** *285* (36), 28044-53.

44. Pearson, A.; Godber, B.; Eisenthal, R.; Taylor, G.; Harrison, R. J. A. S. E., Human milk xanthine dehydrogenase is incompletely converted to the oxidase form in the absence of proteolysis. 2006.

45. Roy, A., A review on the alkaloids an important therapeutic compound from plants. *IJPB* 2017**,** *3* (2), 1-9.

46. Kuramoto, M.; Arimoto, H.; Uemura, D., Bioactive alkaloids from the sea: A review. *Marine drugs* 2004**,** *2* (1), 39-54.

47. Hu, Y.; Chen, J.; Hu, G.; Yu, J.; Zhu, X.; Lin, Y.; Chen, S.; Yuan, J., Statistical research on the bioactivity of new marine natural products discovered during the 28 years from 1985 to 2012. *Marine drugs* 2015**,** *13* (1), 202-221.

48. Zea, S., Henkel, T.P., ; Pawlik, J. R. a picture guide to Caribbean sponges. . Available online at www.spongeguide.org (accessed Accessed on: 2025-05-29).

49. de Voogd, N. J., World Porifera Database. . (2025). .

50. Florent, R. K., Florent's Guide to the Florida, Bahamas & Caribbean Reefs. .

51. Kelly, M.; Bell, L. J.; Herr, B., *Splendid sponges of Palau*. NIWA: 2016.

52. Schupp, P.; Eder, C.; Paul, V.; Proksch, P., Distribution of secondary metabolites in the sponge Oceanapia sp. and its ecological implications. *Marine Biology* 1999**,** *135* (4), 573-580.

53. Neto, C. S.; Nascimento, E.; Cavalcanti, T.; Pinheiro, U., Oceanapia magna sp. nov. (Demospongiae: Tetractinellida: Phloeodictyidae), a new sponge species from the Saint Peter and Saint Paul Archipelago, Brazil. Zootaxa, . 2018, https://doi.org/10.11646/zootaxa.4455.2.6, 4455(2), 289–296. .

54. Singh, K. S.; Das, B.; Naik, C. G., Quinolizidines alkaloids: Petrosin and xestospongins from the sponge Oceanapia sp. *Journal of Chemical Sciences* 2011**,** *123* (5), 601-607.

55. Goud, T. V.; Reddy, N. S.; Swamy, N. R.; Ram, T. S.; Venkateswarlu, Y., Anti-HIV active petrosins from the marine sponge Petrosia similis. *Biological and Pharmaceutical Bulletin* 2003**,** *26* (10), 1498-1501.

56. Dung, D. T.; Hang, D. T. T.; Yen, P. H.; Quang, T. H.; Nhiem, N. X.; Tai, B. H.; Minh, C. V.; Kim, Y.-C.; Kim, D. C.; Oh, H., Macrocyclic bis-quinolizidine alkaloids from Xestospongia muta. *Natural Product Research* 2019**,** *33* (3), 400-406.

57. Kijjoa, A.; Wattanadilok, R.; Campos, N.; Nascimento, M. S. J.; Pinto, M.; Herz, W., Anticancer activity evaluation of kuanoniamines A and C isolated from the marine sponge Oceanapia sagittaria, collected from the Gulf of Thailand. *Marine drugs* 2007**,** *5* (2), 6-22.

58. Carroll, A. R.; Ngo, A.; Quinn, R. J.; Redburn, J.; Hooper, J. N. A., Petrosamine B, an Inhibitor of the Helicobacter p ylori Enzyme Aspartyl Semialdehyde Dehydrogenase from the Australian Sponge Oceanapia sp. *Journal of natural products* 2005**,** *68* (5), 804-806.

59. Xu, M.-J.; Zhong, L.-J.; Chen, J.-K.; Bu, Q.; Liang, L.-F., Secondary metabolites from marine sponges of the genus Oceanapia: chemistry and biological activities. *Marine drugs* 2022**,** *20* (2), 144.

60. Uriz, M. J.; Garate, L.; Agell, G., Molecular phylogenies confirm the presence of two cryptic Hemimycale species in the Mediterranean and reveal the polyphyly of the genera Crella and Hemimycale (Demospongiae: Poecilosclerida). *PeerJ* 2017**,** *5*, e2958.

61. Garate Amenabarro, L., Growth and dynamics of Hemimycale columella. 2017.

62. Let, J.; Donadey, C.; Froget, C., The calcium carbonate spherules of Hemimycale columella (Demosponges, Poecilosclerida) and their taxonomic value. *Taxonomy of Porifera* 1987, 259.

63. Puglisi, M. P.; Sneed, J. M.; Ritson-Williams, R.; Young, R., Marine chemical ecology in benthic environments. *Natural Product Reports* 2019**,** *36* (3), 410-429.

64. Marmouzi, I.; Ezzat, S. M.; Mostafa, E. S.; El Jemli, M.; Radwan, R. A.; Faouzi, M. E. A.; Tamsouri, N.; Kharbach, M., Isolation of secondary metabolites from the mediterranean sponge species; Hemimycale columella and its biological properties. *SN Applied Sciences* 2021**,** *3* (2), 207.

65. Hartiadi, L.; Rebecca, J.; Sheryl, S.; Crystalia, A. A., A Review on the Antimicrobial Properties of Giant Barrel Sponge-Xestospongia sp. *Indonesian Journal of Life Sciences* 2020, 96-112.

66. Maldonado, M.; Aguilar, R.; Bannister, R.; Bell, J.; Conway, J.; Dayton, P.; Díaz, C.; Gutt, J.; Kelly, M.; Kenchington, E., Sponge grounds as key marine habitats: a synthetic review of types, structure, functional roles, and conservation concerns. *Marine animal forests: The ecology of benthic biodiversity hotspots* 2017.

67. Łukowiak, M.; Van Soest, R.; Klautau, M.; Pérez, T.; Pisera, A.; Tabachnick, K., The terminology of sponge spicules. *Journal of Morphology* 2022**,** *283* (12), 1517-1545.

68. Vu Luu, P.; Minh Nguyen, H.; Minh Phan, P.; Duy Vo, A.; Ton-Nu, H. L., Testusterol, a new sterol of the sponge species Xestospongia testudinaria from Phu Quoc island, Vietnam. *Natural Product Research* 2024, 1-9.

69. El-Gamal, A. A.; Al-Massarani, S. M.; Shaala, L. A.; Alahdald, A. M.; Al-Said, M. S.; Ashour, A. E.; Kumar, A.; Abdel-Kader, M. S.; Abdel-Mageed, W. M.; Youssef, D. T., Cytotoxic Compounds from the Saudi Red Sea Sponge Xestospongia testudinaria. *Marine drugs* 2016, *14* (5).

70. Khodzori, F. A.; Mazlan, N. B.; Chong, W. S.; Ong, K. H.; Palaniveloo, K.; Shah, M. D., Metabolites and Bioactivity of the Marine Xestospongia Sponges (Porifera, Demospongiae, Haplosclerida) of Southeast Asian Waters. *Biomolecules* 2023, *13* (3).

71. Quah, Y.; Mohd Ismail, N. I.; Ooi, J. L. S.; Affendi, Y. A.; Abd Manan, F.; Wong, F.-C.; Chai, T.-T., Identification of novel cytotoxic peptide KENPVLSLVNGMF from marine sponge Xestospongia testudinaria, with characterization of stability in human serum. *International Journal of Peptide Research and Therapeutics* 2018, *24*, 189-199.

72. Li, D.; Xu, Y.; Shao, C.-L.; Yang, R.-Y.; Zheng, C.-J.; Chen, Y.-Y.; Fu, X.-M.; Qian, P.-Y.; She, Z.-G.; Voogd, N. J. d.; Wang, C.-Y. Antibacterial Bisabolane-Type Sesquiterpenoids from the Sponge-Derived Fungus Aspergillus sp *Marine drugs* [Online], 2012, p. 234-241.

73. Rose, Y.; Duarte, J. M.; Lowe, R.; Segura, J.; Bi, C.; Bhikadiya, C.; Chen, L.; Rose, A. S.; Bittrich, S.; Burley, S. K. J. J. o. m. b., RCSB Protein Data Bank: architectural advances towards integrated searching and efficient access to macromolecular structure data from the PDB archive. 2021, *433* (11), 166704.

74. Kim, S.; Chen, J.; Cheng, T.; Gindulyte, A.; He, J.; He, S.; Li, Q.; Shoemaker, B. A.; Thiessen, P. A.; Yu, B. J. N. a. r., PubChem 2023 update. 2023, *51* (D1), D1373-D1380.

75. Dulsat, J.; López-Nieto, B.; Estrada-Tejedor, R.; Borrell, J. I. J. M., Evaluation of free online ADMET tools for academic or small biotech environments. 2023, *28* (2), 776.

76. El-Hachem, N.; Haibe-Kains, B.; Khalil, A.; Kobeissy, F. H.; Nemer, G. J. N. M.; Protocols, AutoDock and AutoDockTools for protein-ligand docking: beta-site amyloid precursor protein cleaving enzyme 1 (BACE1) as a case study. 2017, 391-403.

77. Krause, F.; Voigt, K.; Di Ventura, B.; Öztürk, M. A. J. F. i. M. B., ReverseDock: a web server for blind docking of a single ligand to multiple protein targets using AutoDock Vina. 2023**,** *10*, 1243970.

78. Visualizer, D. S., Discovery Studio Visualizer. 2. *Accelrys software inc* 2005.

79. Chandrasekaran, B.; Abed, S. N.; Al-Attraqchi, O.; Kuche, K.; Tekade, R. K., Computer-aided prediction of pharmacokinetic (ADMET) properties. In Dosage form design parameters, Elsevier: (2018), pp 731-755.

80. Perrine, Z. Cyanotoxines et barrière intestinale humaine: Étude comparée de l'absorption et de la toxicité de deux variants de microcystine sur le modèle cellulaire Caco-2. Agrocampus-Ecole nationale supérieure d'agronomie de rennes, 2011.

81. Waters, L. J.; Shokry, D. S.; Parkes, G. M.; Mitchell, J. C. J. J. o. p. s., The use of bile salt micelles for the prediction of human intestinal absorption. 2016**,** *105* (12), 3611-3614.

82. Amin, M. L. J. D. t. i., P-glycoprotein inhibition for optimal drug delivery. 2013**,** *7*, DTI. S12519.

83. Gosselet, F.; Candela, P.; Cecchelli, R.; Fenart, L. J. m. s., La barrière hémato-encéphalique-Une nouvelle cible thérapeutique dans la maladie d'Alzheimer? 2011**,** *27* (11), 987-992.

84. Volpe, D. A. J. F. m. c., Drug-permeability and transporter assays in Caco-2 and MDCK cell lines. 2011**,** *3* (16), 2063-2077.

85. Kratochwil, N. A.; Huber, W.; Müller, F.; Kansy, M.; Gerber, P. R. J. B. p., Predicting plasma protein binding of drugs: a new approach. 2002**,** *64* (9), 1355-1374.

86. Lynch, T.; Price, A. J. A. f. p., The effect of cytochrome P450 metabolism on drug response, interactions, and adverse effects. 2007**,** *76* (3), 391-396.

87. Thomas, D. N.; Wills, J. W.; Tracey, H.; Baldwin, S. J.; Burman, M.; Williams, A. N.; Harte, D. S.; Buckley, R. A.; Lynch, A. M. J. M., Ames test study designs for nitrosamine mutagenicity testing: qualitative and quantitative analysis of key assay parameters. 2024**,** *39* (2), 78-95.

88. van der Laan, J. W.; Kasper, P.; Silva Lima, B.; Jones, D. R.; Pasanen, M. J. C. R. i. T., Critical analysis of carcinogenicity study outcomes. Relationship with pharmacological properties. 2016**,** *46* (7), 587-614.

89. Jing, Y.; Easter, A.; Peters, D.; Kim, N.; Enyedy, I. J., In silico prediction of hERG inhibition. *Future medicinal chemistry* 2015**,** *7* (5), 571-586.

90. Fan, J.; Fu, A.; Zhang, L., Progress in molecular docking. *Quantitative Biology* 2019**,** *7*, 83-89.

91. Shuvo, A. U. H.; Alimullah, M.; Jahan, I.; Mitu, K. F.; Rahman, M. J.; Akramuddaula, K.; Khan, F.; Dash, P. R.; Subhan, N.; Alam, M. A., Evaluation of Xanthine Oxidase Inhibitors Febuxostat and Allopurinol on Kidney Dysfunction and Histological Damage in Two-Kidney, One-Clip (2K1C) Rats. *Scientifica* 2025**,** *2025*, 7932075.

92. Adjadj, M.; Baghiani, A., Propriétés antioxydantes et activité inhibitrice de la Xanthine oxydase des extraits de la plante médicinale Ajuga iva (L.) Schreber. 2009.

93. Habte, M. L.; Beyene, E. A., Biological application and disease of oxidoreductase enzymes. In Oxidoreductase, IntechOpen: (2020).

94. Kumar, R.; Darpan; Sharma, S.; Singh, R., Xanthine oxidase inhibitors: a patent survey. *Expert opinion on therapeutic patents* 2011**,** *21* (7), 1071-108.

95. Liu, N.; Xu, H.; Sun, Q.; Yu, X.; Chen, W.; Wei, H.; Jiang, J.; Xu, Y.; Lu, W. J. O. M.; Longevity, C., The role of oxidative stress in hyperuricemia and xanthine oxidoreductase (XOR) inhibitors. 2021**,** *2021*.

96. Hille, R. J. M., Xanthine oxidase—a personal history. 2023**,** *28* (4), 1921.

97. Kostić, D. A.; Dimitrijević, D. S.; Stojanović, G. S.; Palić, I. R.; Đorđević, A. S.; Ickovski, J. D. J. J. o. C., Xanthine oxidase: isolation, assays of activity, and inhibition. 2015**,** *2015*.

98. Yamaguchi, Y.; Matsumura, T.; Ichida, K.; Okamoto, K.; Nishino, T. J. J. o. B., Human xanthine oxidase changes its substrate specificity to aldehyde oxidase type upon mutation of amino acid residues in the active site: roles of active site residues in binding and activation of purine substrate. 2007**,** *141* (4), 513-524.

APPENDICES

Appendix 1: 2D structure of uric acid.
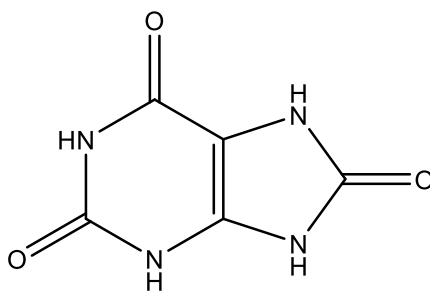
Appendix 2: Structural information on HXO available in the PDB.

PDB Code	Ligands	Resolution	References
2CKJ	FES, FAD, GOL, ACY, PO4	3.59 Å	**[44]**
2E1Q	BCT, FES, FAD, MTE, MOM, SAL, CA	2.6 Å	**[98]**

Appendix 3: Xanthine oxidase reaction mechanism

Hypoxanthine   Xanthine   Acide urique